DIPLOMARBEIT

Assessment of Deadwood Biomass for the Biosphere Reserve Rohrach

zur Erlangung des akademischen Grades

Diplom-Ingenieur/in

ausgeführt am Department für

Geodäsie und Geoinformation

Forschungsbereich Photogrammetrie

der Technischen Universität Wien

unter Anleitung von

Univ.Prof. Dipl.-Ing. Dr.techn. Norbert Pfeifer

und

Dipl.Ing. Dr.techn. Markus Hollaus

durch

Jakob Galle

Matrikelnummer: 11714934

Wien, am [redacted]

Unterschrift (Verfasser/in) Unterschrift (Betreuer/in)

Eidesstaatliche Erklärung

Ich erkläre an Eides statt, dass die vorliegende Arbeit nach den anerkannten Grundsätzen für wissenschaftliche Abhandlungen von mir selbstständig erstellt wurde. Alle verwendeten Hilfsmittel, insbesondere die zugrunde gelegte Literatur, sind in dieser Arbeit genannt und aufgelistet. Die aus den Quellen wörtlich entnommenen Stellen, sind als solche kenntlich gemacht.

Das Thema dieser Arbeit wurde von mir bisher weder im In- noch Ausland einer Beurteilerin/einem Beurteiler zur Begutachtung in irgendeiner Form als Prüfungsarbeit vorgelegt. Diese Arbeit stimmt mit der von den Begutachterinnen/Begutachtern beurteilten Arbeit überein.

Wien, am 

Acknowledgements

I would like to thank everyone who supported me during this master's thesis and throughout my studies. Special thanks go to my supervisor, Markus Hollaus, for his valuable input and guidance, as well as for assisting me with organizational matters.
I am also grateful to Taskin and Yi-Chen for their support during the field measurements and for the exciting trip to Vorarlberg. A special thanks goes to INATURA for enabling this thesis and especially to Anette Herburger for ensuring a smooth process.
Finally, I would like to thank my parents Eva and Andreas, who supported me throughout my entire studies (emotionally and financially), as well as my fellow students, Till and Vinz, with whom I spent countless hours—some more productive than others.

Kurzfassung

Totholz spielt eine entscheidende Rolle in Waldökosystemen, da es die Biodiversität fördert, den Nährstoffkreislauf unterstützt und Kohlenstoff speichert. Trotz seiner Bedeutung bleibt die automatisierte Erkennung und Messung von Totholz eine Herausforderung, insbesondere in naturbelassenen Wäldern mit dichter Vegetation und überlappenden Stämmen. In dieser Arbeit werden vier Methoden zur Erfassung von Totholz im Naturwaldreservat Rohrach verglichen: manuelle Feldmessungen, "Line Interset" Methode, eine bereits entwickelte UAV-basierte Laserscanning-Methode (ULS) und ein neu entwickelter Algorithmus für terrestrisches Laserscanning (TLS). Der TLS-Ansatz nutzt hochauflösende Punktwolken, um liegendes Totholz zu detektieren. Dabei werden potenzielle Stämme anhand geometrischer Merkmale wie Linearität, Oberflächenorientierung und räumlicher Kontinuität identifiziert. Anschließend werden Polynomfunktionen genutzt, um Durchmesser, Länge und Volumen der Segmente zu berechnen. Drei Probeflächen mit einem Radius von 12 Metern wurden untersucht, um die Methoden unter unterschiedlichen Waldbedingungen zu evaluieren. Die ULS-Methode erwies sich als effizient für großflächige Kartierungen, war jedoch weniger effektiv bei der Erkennung kleinerer oder verdeckter Stämme. Der TLS-Ansatz lieferte detailliertere Messungen, hatte jedoch Schwierigkeiten in Gebieten mit sehr dichtem Unterwuchs und überlappenden Strukturen. Manuelle Messungen, obwohl präzise, waren zeitaufwändig und für größere Flächen weniger praktikabel. Die Ergebnisse zeigen, dass jede Methode ihre eigenen Stärken und Schwächen hat. Eine Kombination von ULS- und TLS-Daten könnte eine umfassendere Lösung bieten, indem ULS für großflächige Erfassungen und TLS für detaillierte Analysen genutzt wird. Diese Arbeit leistet einen Beitrag zur Weiterentwicklung von Methoden zur Totholzerkennung und liefert wertvolle Einblicke für das Monitoring von Biodiversität und das Waldmanagement.

Abstract

Deadwood plays an essential role in forest ecosystems by supporting biodiversity, helping to cycle nutrients and storing carbon. Despite its importance, accurately detecting and measuring deadwood remains a challenge, especially in unmanaged forests with dense vegetation and overlapping logs. This study compares four methods for assessing deadwood in the Rohrach biosphere reserve: manual field measurements, the line intersect method, an already developed UAV-based laser scanning (ULS) method, and a newly developed Terrestrial Laser Scanning (TLS) algorithm. The TLS approach uses high-density point clouds to detect lying deadwood. It identifies potential logs by analyzing geometric features such as linearity, surface orientation, and spatial continuity. Polynomial fitting is then applied to estimate the diameter, length, and volume of each segment. The algorithm was designed to handle complex forest structures. Three 12-meter-radius plots were analyzed to evaluate the methods under varying forest conditions. The ULS method was efficient in covering large areas, but was less effective in identifying smaller or obstructed logs. In contrast, the TLS approach provided more detailed measurements, but struggled with heavily vegetated areas and overlapping logs. Manual field measurements, while accurate, were time consuming and less practical for larger areas. The results show that each method has its strengths and limitations. Combining ULS and TLS data may offer a more comprehensive solution, leveraging ULS for wide coverage and TLS for detailed analysis. This study contributes to the development of improved methods for deadwood detection, providing valuable information for biodiversity monitoring and forest management.

Contents

List of Figures

List of Tables

List of Abbreviations

AOI Area of Interest

ALS Airborne Laser Scanning

BEV Bundesamt für Eich- und Vermessungswesen

CWD Coarse Woody Debris

DBH Diameter at Breast Hight

DEM Digital Elevation Model

DTM Digital Terrain Model

GIS Geo Information System

LiDAR Light Detection and Ranging

LS Laser Scanning

MSA Multistation Adjustment

OHM Object Height Model

RANSAC Random Sample Consensus

RMSE Root Mean Square Error

TLS Terrestrial Laser Scanning

UAV Unmanned Arial Vehicle

ULS Unmanned Arial Vehicle Laser Scanning

1. Introduction

1.1. Problem Statement and Relevance

Deadwood, often referred to as coarse woody debris (CWD), is crucial for preserving the health and diversity of forest ecosystems. It supports numerous species and is integral to nutrient cycling, which improves soil fertility and fosters the growth of new vegetation, thus maintaining the forest's overall productivity. Moreover, deadwood acts as a measure of forest management practices and the ecosystem's condition (Merganičová et al., 2012; Stokland et al., 2012). Intensive forest management practices in Europe have historically led to a substantial decrease in deadwood, which in turn has caused a reduction in biodiversity. Acknowledging its critical role, deadwood has been integrated into several forest biodiversity indicators and monitoring initiatives across Europe. The Ministerial Conference on the Protection of Forests in Europe (MCPFE) considers deadwood as one of nine key indicators for sustainable forest management. Likewise, the European Environment Agency (EEA) includes deadwood as one of its principal biodiversity indicators (Humphrey et al., 2005). The Rohrach biosphere reserve is a protected area characterized by its dense and largely unmanaged forest landscapes. Established to conserve the region's natural biodiversity and ecological processes, the reserve encompasses a variety of habitats, including old-growth forests, wetlands, and riparian zones. These diverse environments support a rich array of flora and fauna, many of which are dependent on deadwood for their survival (Grabherr and Broggi, 1999; Kirchmeir et al., 2023). The reserve's management practices emphasize minimal human intervention, allowing natural processes to shape the forest structure. This approach has led to a significant accumulation of deadwood, providing an ideal setting for studying its role in forest dynamics. Historical data on deadwood from the 1990s, collected through manual measurements by Grabherr and Broggi (1999), offer a valuable baseline for understanding changes over time and evaluating the effectiveness of different assessment methods. Despite the recognized importance of deadwood in maintaining forest biodiversity and ecological processes, there is still a significant gap in our understanding of the most effective methods for its assessment in unmanaged forests. Traditional manual measurement techniques, while reliable, are labor-intensive and time-consuming, making it challenging to apply them across large forest areas (Marchi et al., 2018). Recent advancements in remote sensing technologies, such as TLS, ULS and ALS offer promising alternatives that can potentially provide more accurate and efficient assessments of deadwood (Pesonen et al., 2008; Yrttimaa et al., 2020). However, there is a lack of comprehensive studies comparing these modern techniques with conventional methods, particularly in the context of dense and unmanaged forest landscapes like those in the Rohrach biosphere reserve. While historical data on deadwood from the 1990s exist for this reserve, these data have primarily been collected through manual measurements (Grabherr and Broggi, 1999). There have been attempts to combine old data with new remote sensing data to understand long-term changes and check

the accuracy of new methods (Kirchmeir et al., 2023). However, more studies are needed to improve this integration and deepen our understanding of deadwood detection methodologies. Addressing this knowledge gap is crucial for developing standardized protocols for deadwood assessment that are both efficient and accurate. Such protocols are necessary for effective forest management and conservation strategies aimed at preserving biodiversity and ecological integrity (Humphrey et al., 2005). This study aims to fill this gap by systematically comparing conventional manual methods with TLS and ULS.

1.2. Objectives of the Study

The main goal of this study is to compare the effectiveness of different methods in measuring deadwood in dense, unmanaged forests of the Rohrach biosphere reserve. These methods include traditional manual measurements (Line Intersect Method), TLS, and ULS. A new method to derive lying deadwood parameters from TLS point cloud data was developed and tested. This method was specifically designed to improve the detection and measurement of deadwood in complex forest conditions. The study evaluates the accuracy of each method by comparing the results of TLS and ULS with a set of precise control measurements. The aim is to identify the strengths and weaknesses of each method as well as the types of errors that they may introduce. In addition, the study investigates how forest density and structure affect the performance of these methods. Understanding these influences helps identify conditions where certain methods may work better or face limitations. Although guidelines and recommendations for future forest management were planned, the study focuses primarily on evaluating current methods and testing the new TLS-based approach. This provides foundational information to improve deadwood monitoring in unmanaged forests.

1.3. Structure of the Thesis

Chapter 2 **Theoretical background**, explores the ecological significance of deadwood and reviews existing methods for TLS, and ULS while referencing relevant studies. The study area is detailed in Chapter 3, **Study Area**, which describes the unique characteristics of the Rohrach biosphere reserve. This chapter emphasizes its dense forest structure, unmanaged nature, and challenging terrain, all of which influence the choice and performance of measurement methods. Chapter 4, **Methodology**, outlines the data collection and processing techniques used in the study. It describes how manual measurements, TLS, and ULS data were gathered, processed, and analyzed. A significant portion of this chapter is dedicated to explaining the newly developed TLS approach, including the algorithms and criteria used for detecting deadwood in point-cloud data. The outcomes of the study are presented in Chapter 5, **Results**, which compares the performance of the different methods in terms of accuracy, efficiency, and practicality. Special attention is paid to the new TLS method, highlighting its strengths and limitations in identifying and measuring deadwood in complex

forest environments. In Chapter 6, **Discussion**, the results are analyzed with respect to the research objectives. This chapter evaluates the reliability and applicability of the methods, discusses the influence of forest density and structure on their performance, and offers suggestions for improving the TLS approach. Recommendations for the integration of TLS and ULS are also included. Finally, Chapter 7, **Conclusion and Outlook**, summarizes the key findings of the study and highlights its contributions to deadwood assessment research. Practical recommendations for forest managers and researchers are provided, along with proposals for future research, including refining the TLS approach and testing it in diverse forest ecosystems. These insights aim to support the development of more efficient and accurate deadwood monitoring methods for forest conservation and management.

2. Theoretical Background

2.1. Role of Deadwood in Forest Ecosystems

Deadwood is an essential element of forest ecosystems, fulfilling important ecological and structural functions. It encompasses standing dead trees, fallen logs, stumps, and branches, all of which enhance the forest's biodiversity and carbon storage potential. Coarse woody debris (CWD) provides crucial habitat for a variety of species, including fungi, insects, birds, and mammals, many of which are wholly reliant on deadwood for shelter, nesting, and foraging. This reliance is especially evident in saproxylic organisms, like certain beetles and fungi, which depend on decaying wood at specific life stages. Additionally, habitat trees with larger diameters frequently accommodate cavity-nesting birds and small mammals, highlighting the significance of deadwood as a measure of biodiversity (Marchetti, 2004; Merganičová et al., 2012). In addition to its role in biodiversity, deadwood significantly influences nutrient cycling and carbon storage in forest ecosystems. As it decomposes, it reintroduces essential nutrients such as nitrogen, phosphorus, calcium, and magnesium back into the soil, benefiting the forest floor and promoting plant growth. Furthermore, deadwood acts as a temporary carbon repository, where its gradual decay moderates carbon dioxide emissions, aiding in climate change mitigation. The amount of carbon retained in deadwood varies considerably among ecosystems, affected by forest management strategies and natural occurrences. (Merganičová et al., 2012; Paletto et al., 2012). Furthermore, deadwood serves as an indicator of forest management practices and ecosystem health. Its presence and abundance often reflect the naturalness of a forest and the extent of human impacts, such as logging or land-use changes. Consequently, accurate assessment and monitoring of deadwood are critical for developing effective conservation and management strategies (Merganičová et al., 2012; Stokland et al., 2012). The dimensions of deadwood, including diameter, length, and height, play a pivotal role in its ecological functions. Larger pieces, particularly those exceeding 30 cm in diameter, are critical habitats for diverse species, providing shelter, nesting sites, and foraging opportunities. Moreover, precise measurements of these parameters are essential for accurately estimating deadwood volume, a key factor in ecological and carbon studies. The volume, calculated using mid-diameter and length, reflects the biomass and its potential contributions to the nutrient and carbon cycles (Marchetti, 2004; Merganičová et al., 2012; Paletto et al., 2012). The continuity of deadwood in both space and time is of equal importance. How deadwood is spread throughout a forest influences both the habitats available and the processes within the ecosystem. An even and constant distribution of deadwood provides ongoing resources for species at various stages of decay. Moreover, the timing of deadwood addition, including regular recruitment, is essential to uphold ecological functions over time. This highlights the importance of implementing deadwood management practices that support the ecosystem's long-term stability (Marchetti, 2004; Merganičová et al., 2012; Paletto et al., 2012). Structurally, deadwood contributes to soil stabilization, particularly in

steep or erosion-prone areas. Fallen logs can slow down water and soil movement, reducing erosion on slopes and aiding in water retention. In addition, they can protect against avalanches and rockfalls, especially in mountainous regions. Over time, as the wood decomposes, this protective role diminishes, highlighting the dynamic nature of deadwood in forest ecosystems (Paletto et al., 2012). Historically, intensive forest management in Europe has significantly reduced the amount of deadwood, leading to a decline in biodiversity. Managed forests typically contain much less deadwood compared to natural forests. Recognizing its ecological importance, deadwood has been incorporated into biodiversity indicators and monitoring programs across Europe (Marchetti, 2004). However, the quantity and quality of deadwood are often affected by forest management practices. In intensively managed forests, deadwood is frequently removed to reduce the risk of pests, diseases, and fires, leading to significantly lower volumes compared to natural or semi-natural forests. Conversely, biodiversity-oriented forest management aims to maintain or increase deadwood levels to bridge the gap between managed and unmanaged forests. The balance between maintaining ecological benefits and addressing management costs, such as pest control and fire hazards, remains a central challenge in sustainable forestry (Marchetti, 2004; Merganičová et al., 2012). Overall, deadwood is not only a vital component for maintaining biodiversity and supporting ecosystem functions but also a crucial element in sustainable forest management strategies. Its ecological, structural, and carbon storage roles underscore its importance, particularly in efforts to conserve forest ecosystems and combat climate change.

2.2. Methods for Determining Deadwood

2.2.1. UAV Laser Scanning (ULS) and Airborne Laser Scanning (ALS)

UAV and Airborne laser scanning have proven to be a highly effective tool for identifying deadwood due to its ability to collect high-resolution LiDAR data over small and complex forest areas. Various methods have been developed to analyze CWD and fallen logs from ULS/ALS point clouds, combining geometric, spatial, and machine-learning techniques to address challenges such as dense vegetation, fragmented logs, and ground-level interference (Polewski et al., 2015). A commonly used method is line template matching, which identifies linear structures in point clouds that correspond to fallen tree stems. This approach examines the alignment and dimensions of potential objects, making it particularly suitable for detecting larger logs. In contrast, Lindberg et al. (2013) utilized ALS data, which, despite being collected over larger areas, provided exceptionally high point density. This enabled the detection of fallen tree stems with a level of detail comparable to ULS datasets. The high point density in ALS data significantly enhanced the identification of linear structures and supported the accurate analysis of fallen logs, even in challenging forest conditions. However, like ULS-based methods, line template matching applied to ALS data faced challenges in environments with dense understory vegetation or when deadwood was broken into smaller

fragments. A more advanced method is the "Normalized Cut" approach, which applies machine learning to segment point clouds into individual logs or tree stems. By analyzing the three-dimensional geometric properties of each segment, this method can group related points together, enabling the identification of fragmented or partially visible deadwood. By training on both simulated and real datasets, the approach achieves higher robustness and accuracy, even in forests with dense vegetation. Its adaptability to different forest conditions makes it one of the more versatile techniques for deadwood detection using ALS (Polewski et al., 2015). Nyström et al., 2014 subtracted a standard DEM from a detailed DEM and created an Object Height Model (OHM), highlighting objects close to the ground. Template matching was then applied to the OHM to detect windthrown trees by correlating rectangular templates of various sizes and orientations with the data. This approach facilitated the detection of individual windthrown trees, even in areas with canopy cover. Voxel-based filtering is another promising approach, dividing point clouds into small three-dimensional cubes (voxels) and analyzing their density and height to isolate ground-level features. This method focuses on identifying structures close to the ground, such as lying logs, while filtering out canopy layers and other noise. By doing so, voxel-based filtering enhances the ability to detect fallen logs in forests with complex structures or dense vegetation (Kirchmeir et al., 2023). Mücke et al., 2012 developed a method for detecting downed deadwood in high-resolution ALS data, combining point cloud filtering, morphological image processing, and echo parameter analysis. By applying height and echo width filters alongside additional statistical criteria, fallen tree stems were reliably identified as elongated structures. The method generates vector data that serve as a foundation for further analyses. Despite the significant progress made in developing these methods, challenges remain. Dense vegetation and fragmented deadwood often reduce detection accuracy, while noise in ULS and ALS point clouds requires robust filtering and segmentation techniques. The effectiveness of ULS and ALS methods is also influenced by factors such as flight altitude, sensor configuration, and environmental conditions, which can affect the resolution and quality of the data collected. Nevertheless, combining multiple approaches, such as line template matching with machine learning or integrating orthophotos with LiDAR, has been shown to improve the reliability of the methods across diverse forest environments (Nyström et al., 2014; Pesonen et al., 2008; Polewski et al., 2015). In conclusion, ULS and ALS are a powerful and flexible tool for mapping deadwood. Advances in algorithms and the integration of complementary datasets are continuously improving its efficiency and accuracy, establishing it as a critical technology for forest management and biodiversity research.

2.2.2. Terrestrial Laser Scanning (TLS)

Terrestrial laser scanning (TLS) has revolutionized forest research by providing detailed three-dimensional point clouds that capture the structure and composition of forest environments with exceptional accuracy. Traditionally, TLS has been used for tasks such as mea-

suring tree attributes, including diameter at breast height (DBH), tree height, stem volume, and biomass. Additionally, it has been employed to analyze canopy structures, assess forest dynamics, and even evaluate timber quality. These capabilities make TLS an invaluable tool for forest inventory and monitoring, offering a non-destructive and precise alternative to conventional field-based methods. With ongoing advancements in scanner technology, data processing algorithms, and computational capacity, TLS has extended its utility to include the detection and characterization of deadwood, a crucial yet understudied component of forest ecosystems (Liang et al., 2018; Yrttimaa et al., 2019; Yrttimaa et al., 2020). However, detecting and quantifying CWD remains challenging due to its variability in size, orientation, and degree of decomposition. Unlike standing deadwood, which is structurally similar to living trees and can be identified more easily, lying deadwood often lacks consistent geometric features, making its detection more complex. Methods such as Random Sample Consensus (RANSAC) are commonly used for identifying cylindrical shapes, and while they have been adapted to detect certain deadwood features, their effectiveness is often limited by dense canopy cover or overlapping vegetation, which obstructs accurate data acquisition and processing (Yrttimaa et al., 2019; Yrttimaa et al., 2020). The detection of downed deadwood is considerably more complex due to its position near or on the forest floor, where it is often hidden by understory vegetation, leaf litter, or soil. To address these challenges, researchers have developed multi-step workflows that combine statistical modeling, raster-based segmentation, and advanced classification techniques. For instance, Polewski et al., 2017 introduced a voting-based statistical cylinder detection framework that utilizes continuous parameter spaces and kernel density estimation to improve the detection of fallen logs in complex forest environments. This method enhances the accuracy of deadwood delineation by focusing on geometric features specific to logs, such as their cylindrical structure and alignment on the ground. Despite these advancements, several challenges remain. Dense vegetation and occlusions often result in incomplete point clouds, particularly for small-diameter logs or logs in advanced decay stages. This can lead to underestimation of total deadwood volume. Additionally, the reliance on multi-scan setups, which are necessary to minimize occlusions, increases the time and effort required for fieldwork and data processing. Automating the detection and classification of deadwood also presents significant difficulties, especially in complex forest environments with overlapping or fragmented logs. Furthermore, while TLS provides unparalleled detail for small plots, scaling this approach to larger areas remains a logistical and computational challenge (Liang et al., 2018; Yrttimaa et al., 2019; Yrttimaa et al., 2020). To address these limitations, recent research has explored the integration of TLS with other remote sensing technologies, such as UAV-based photogrammetry and airborne LiDAR. These combined approaches have the potential to overcome some of the spatial and logistical constraints of TLS by leveraging the strengths of multiple data sources. For example, UAVs can cover larger areas efficiently, providing context for TLS data, while TLS captures finer details that are often missed by airborne sen-

sors. This synergy could enable more comprehensive deadwood mapping, enhancing our understanding of its ecological and structural roles in forest ecosystems (Marchi et al., 2018; Yrttimaa et al., 2019). In summary, TLS has demonstrated significant potential for detecting and characterizing deadwood in forest environments, offering precise measurements of key attributes such as volume, dimensions, and spatial distribution. However, its effectiveness is currently limited by challenges related to occlusion, automation, and scalability. Addressing these limitations through algorithmic improvements and multi-sensor integration could pave the way for operationally viable TLS-based methods, complementing traditional forest inventory practices and advancing ecological research.

3. Study Area

3.1. Description of the Rohrach Biosphere Reserve

The Rohrach Forest, a 47.5-hectare natural area located in Vorarlberg, Austria near the Austrian-German border, serves as the study site for this research (Figure 3.1). This forest was designated as a biosphere forest reserve in 1992 under regional conservation laws, with the primary goal of allowing natural processes to unfold without human interference. Unlike traditional forest management, this designation ensures that no forestry activities or geomorphological interventions occur within the reserve. Such measures aim to create an untouched forest ecosystem that can serve as a baseline for ecological studies. Despite its protected status, certain interventions are allowed under specific circumstances. For example, pest control measures can be implemented to protect surrounding forests, and regulated hunting is permitted to prevent ungulate overpopulation, which could otherwise hinder the natural regeneration of tree species. However, hunting for other wildlife is strictly prohibited. The reserve's initial protection period of 30 years was extended in 2022 for another 30 years, reflecting the long-term commitment to preserving this area. Compensation agreements with landowners were part of the establishment of the reserve. Adjacent forest areas in Germany, covering 177.5 hectares, were similarly designated as protected zones in 1992. However, the management approach there differs, allowing limited forestry, agriculture, hunting and fishing. Additionally, both the Austrian and German portions of the Rohrach Forest were integrated into the Natura 2000 network as Habitat Directive sites, Austria in 1992 and Germany in 2000. This inclusion emphasizes the importance of the area for biodiversity conservation on an european scale. While some parts of the German forest remain under active use, others are designated as non-utilized zones, creating a complex landscape of protection and use. This combination of strict protection measures and limited human activities highlights the diverse strategies employed across national borders to balance conservation with practical considerations. The Rohrach forest thus provides a unique opportunity to study the dynamics of natural forests under varying management regimes (Kirchmeir et al., 2023).
The Rohrach biosphere forest reserve is located in the Alpine foothills. It is characterized by steep gorges carved by streams such as the Loimelesbach, Rickenbach, and Forstbach, which define its boundaries to the west, east, and north. To the south, the area is bordered by a prominent escarpment. The rugged terrain of the reserve alternates between steep slopes, narrow plateaus, and small flat areas, making it difficult to access. Additional streams, including the Kessellochbach and Gruebtobelbach, divide the slopes into three distinct sections. Elevations range from the valley floor to a peak of 720 meters above sea level, resulting in a total height difference of approximately 180 meters. Geologically, the reserve is part of the Molasse Zone, a region formed by sedimentary deposits carried from the Alps during their formation. This unique composition includes alternating layers of permeable and impermeable material, which contribute to water seepage and wet zones in certain ar-

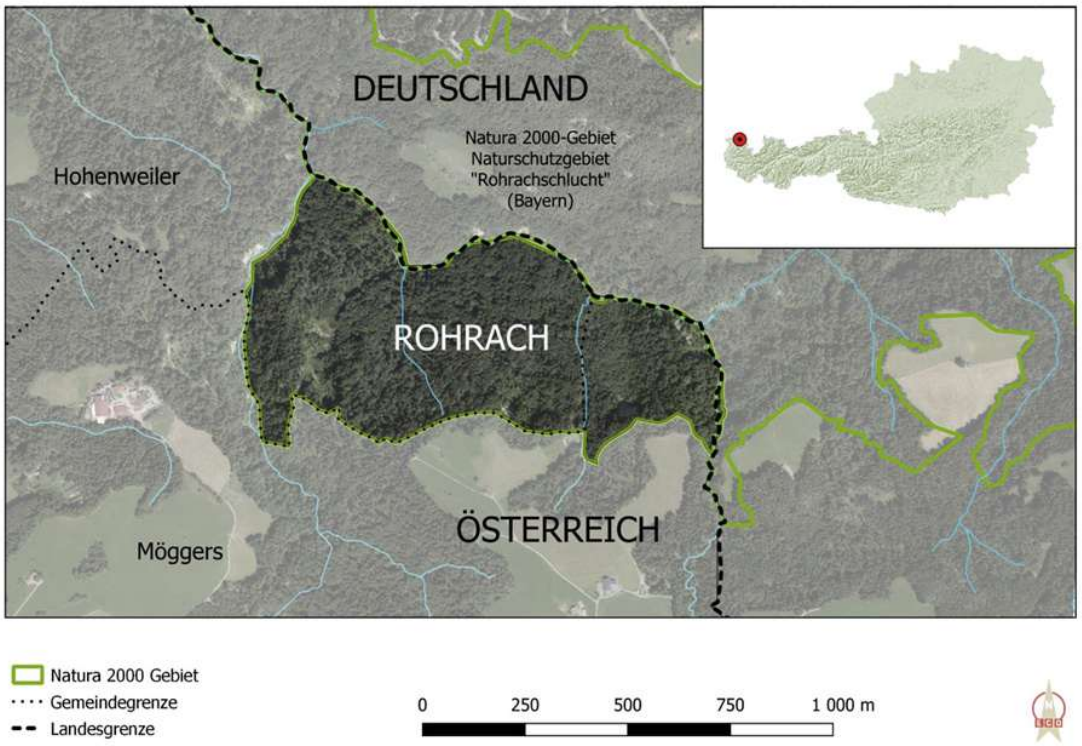

Figure 3.1: Biosphere Reserve Rohrach in the Austrian province Vorarlberg (Kirchmeir et al., 2023)

eas. Over time, these conditions, combined with rapid rock weathering, have led to frequent landslides of various sizes. The dynamic interaction of geological processes shapes the landscape and influences the ecological characteristics of the area (Grabherr and Broggi, 1999). The composition of the terrain reveals a diverse structure. The mid slopes dominate the reserve, covering 36% of the area, while the gentle slopes account for 28%, and the lower slopes represent 18%. Upper slopes make up only 8%, with ridges, rocky outcrops, and other minor features occupying smaller portions. The average elevation across the reserve is approximately 630 meters, with most slopes facing north, 41% oriented toward the north, 21% northeast, and 18% northwest. The general average slope is calculated at 40%, highlighting the steepness of the terrain (Grabherr and Broggi, 1999).

3.2. Study Sites

For the TLS campaign, three pre-surveyed plots were selected: Plot 610, Plot 611, and the permanent observation area D3. These plots were chosen to represent a variety of terrain types and structural challenges, allowing a comprehensive evaluation of the methods applied.

Plot 610 is located on relatively flat terrain, characterized by dense undergrowth and a high density of small trees. Fallen deadwood in this area is often scattered in a criss-cross pat-

tern, with varying states of decay, making it an ideal site to test segmentation and volume estimation techniques. In contrast, plot 611 is on a steep slope, where the terrain causes complications in scanning and data processing. The inclined positioning of some logs also presents challenges in accurately estimating their length and volume.
Plot D3 was selected for its distinctive arrangement of deadwood. A large fallen tree dominates the site, with another substantial log resting on top of it and a smaller log situated nearby. This arrangement allows for testing the robustness of segmentation and volume estimation under complex conditions.

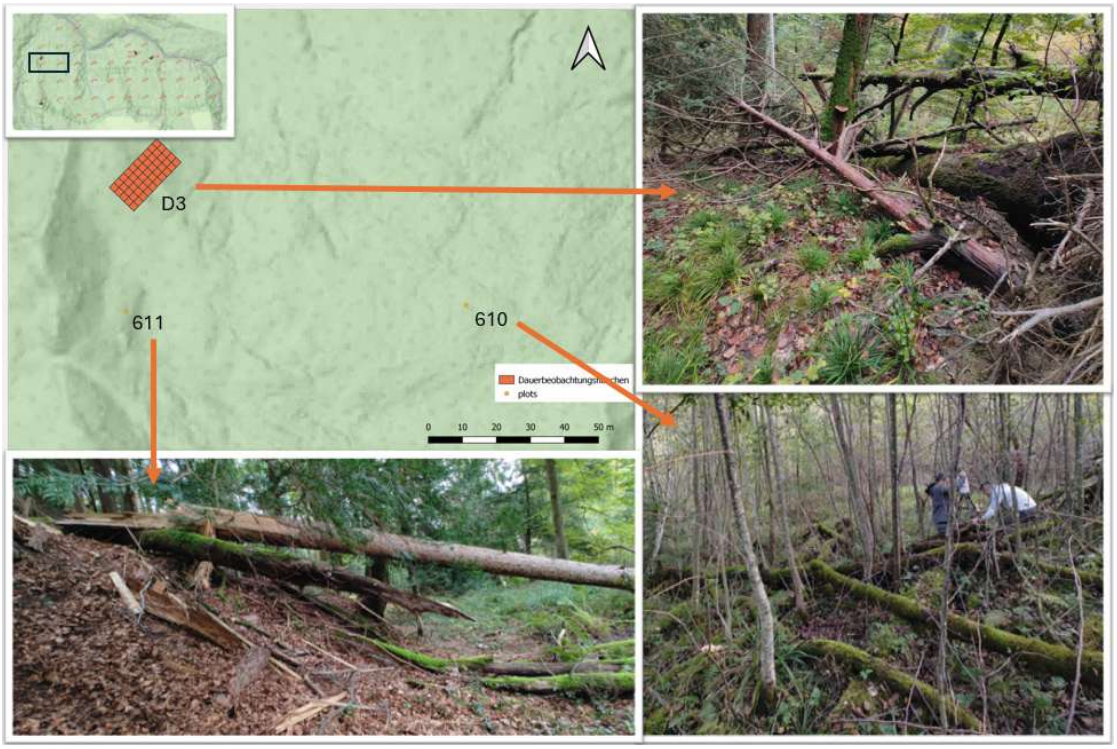

Figure 3.2: Study Area Rohrach. The three chosen plots 610, 611 and D3

Across the three plots, a total of 87 scan positions were used: 35 in Plot 610, 34 in Plot 611, and 18 in Plot D3. These plots collectively represent a diverse range of forest conditions, allowing an in-depth analysis of the strengths and limitations of the methods applied in this study.

4. Methodology

4.1. Data Collection

4.1.1. TLS Data Collection and Point Cloud Registration

The terrestrial laser scanning (TLS) survey was conducted at three sites: D3, 610, and 611, using the RIEGL VZ-600i instrument. Data acquisition for plot 611 included 36 scan positions to ensure complete coverage of the area, while plot 610 required 35 scan positions, and Plot D3 was covered with 18 scan positions. The scans were registered into a global coordinate system (ETRS89/Geocentric) and transformed into a locally leveled Cartesian coordinate system (east, north, up) for analysis.

The scanning process used overlapping scan positions to enhance the precision of point cloud registration. Each scan captured a full 360° horizontal field of view, with an angular resolution of 34 millidegrees. The total number of points collected across all plots exceeded several billion, ensuring high-density coverage of the surveyed areas.

After the scans were registered, a multistation adjustment (MSA) was performed to refine the alignment of individual scans. This process optimized the relative positioning of the scan stations by minimizing residual errors in the point clouds. According to the MSA report for plot 611, the average residual error of the registered points was approximately 2 millimeters, with local adjustments to the scan positions typically remaining below 1 centimeter. This level of accuracy ensures that the TLS data provide a reliable foundation for subsequent analyses.

Despite these efforts, the MSA process highlighted some challenges, including potential outliers in GNSS measurements and variations in residuals. These were addressed by refining parameters, such as the adjustment effort and removing low-trust GNSS observations from the process.

4.1.2. ULS Data Collection

A 48-hectare study area was surveyed using an unmanned aerial vehicle equipped with a LiDAR system and a high resolution camera. The setup featured a RIEGL VUX-120 LiDAR scanner and a PhaseOne iXM100 camera, mounted on a Soleon LasCO 2 multicopter. The flights were carried out by Alto Drones, a company based in South Tyrol, during April 2022 under 'leaf-off' conditions. The resulting 3D point clouds were processed in the ETRS89/UTM32 coordinate system, with orthometric heights derived from the geoid model provided by the Austrian Federal Office for Calibration and Surveying (BEV). These data files were saved in the *.laz format (Kirchmeir et al., 2023).

The study area was scanned using parallel and overlapped flight paths, complemented by cross-strips to improve georeferencing accuracy (Figure 4.1). From the processed 3D point clouds, a Digital Terrain Model (DTM) was computed using the last-return echoes. This step

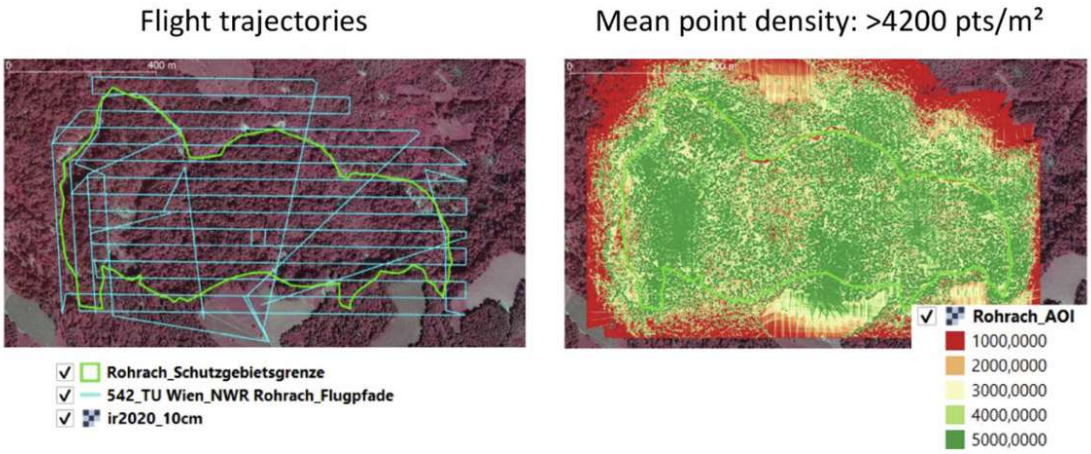

Figure 4.1: UAV Flight Trajectories and Point Density over the Nature Reserve Rorach (Kirchmeir et al., 2023)

was also handled by Alto Drones. The final DTM, delivered in *.tif format, has a spatial resolution of 0.25 x 0.25 meters (Kirchmeir et al., 2023).
The lying deadwood was identified using a decision tree based on normalized 3D point data. This method relied on both the shape and the radiometric characteristics of the LiDAR points. Only logs within 5 meters above ground level were included in the analysis. To estimate the volume, a voxel-based method was used. The diameters of the logs were first measured from 2D raster maps and then used to calculate the volume, with voxel sizes of 5x5x5 cm^3 see Figure 4.2.
This method generally worked well, but some limitations were identified. It faced challenges in areas with overlapping logs or gaps in the LiDAR data, which were often caused by shadowing. Furthermore, the method measured only horizontal distances, which led to an underestimation of volume in steep terrain (Kirchmeir et al., 2023).

4.1.3. Line Intersect Method

The Line Intersect Method is a widely used and efficient approach to estimate the volume of lying deadwood. Originally developed in North America to assess the potential for fire hazard of underbrush (Wagner, 1968), it has since been adapted for various ecological and forestry studies. This method involves imaginary transect lines, along which all deadwood fragments intersecting that exceed a predefined diameter are recorded at the crossing point (Figure 4.3). The technique does not require logs to lie flat on the ground; elevated fragments, such as fallen branches or sections of a tree crown, are also included if they intersect the transect line. Leaning dead trees, tilted more than 45° from the vertical axis, are similarly considered as lying deadwood when they cross the transect (Kirchmeir et al., 2023).
For an accurate volume estimation, two transects, each 40 meters in length, are typically established per plot. These transects intersect at the center of the plot and are oriented to

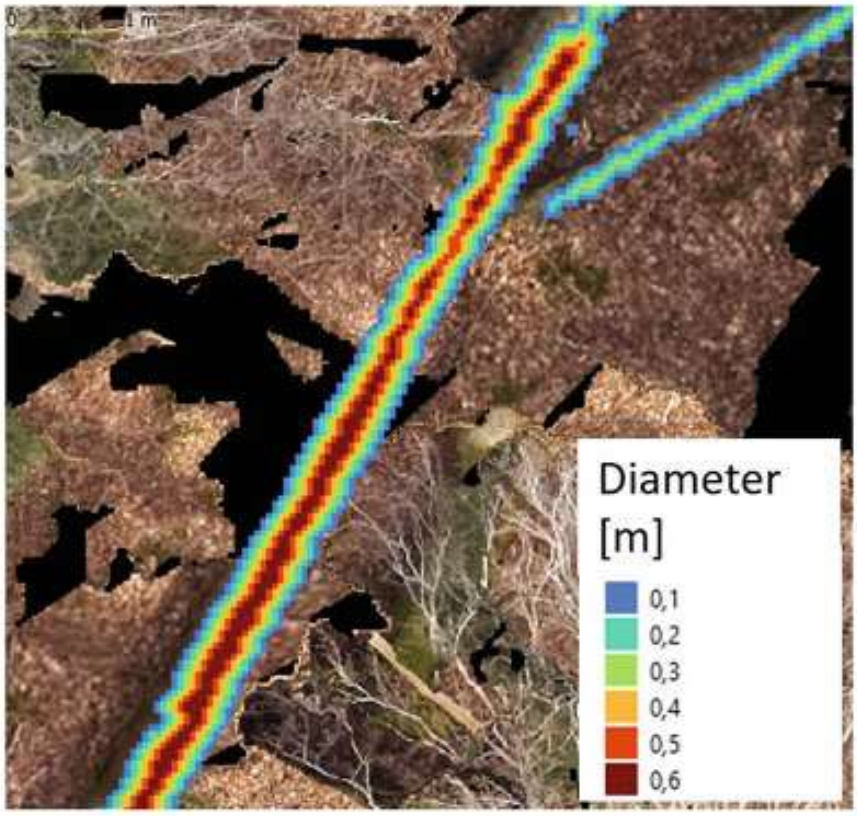

Figure 4.2: Lying Deadwood detected through ULS: derived diameters of lying deadwood stems (Kirchmeir et al., 2023)

suit the terrain. In sloped areas, one transect follows the slope, while the other aligns perpendicular to it, ensuring comprehensive sampling. On flat terrain, transects are commonly oriented along the north-south and east-west directions. If terrain conditions make certain areas inaccessible, the transect lengths may be reduced accordingly, and these adjustments are accounted for in the calculations. In sloped terrain, the recorded distances are corrected to represent horizontal distances, ensuring consistent and comparable results.

At each intersection point, several parameters are measured, including the diameter of the log, species classification (or a broader category such as coniferous, deciduous, or indeterminate for highly decomposed logs), decay stage (categorized into five classes), and the origin of the fragment (e.g. broken, sawn, or wind thrown). For wind thrown logs, the presence of a root plate or exposed roots is used as an identifying feature.

Although the Line Intersect Method provides a time-efficient means of estimating deadwood volume, it has some limitations. The method only accounts for logs that intersect the transect lines, which may lead to under-representation in areas with sparse deadwood distribution. However, it remains a useful approach to derive reference values and compare estimates obtained by more advanced techniques, such as terrestrial laser scanning (Kirchmeir et al., 2023).

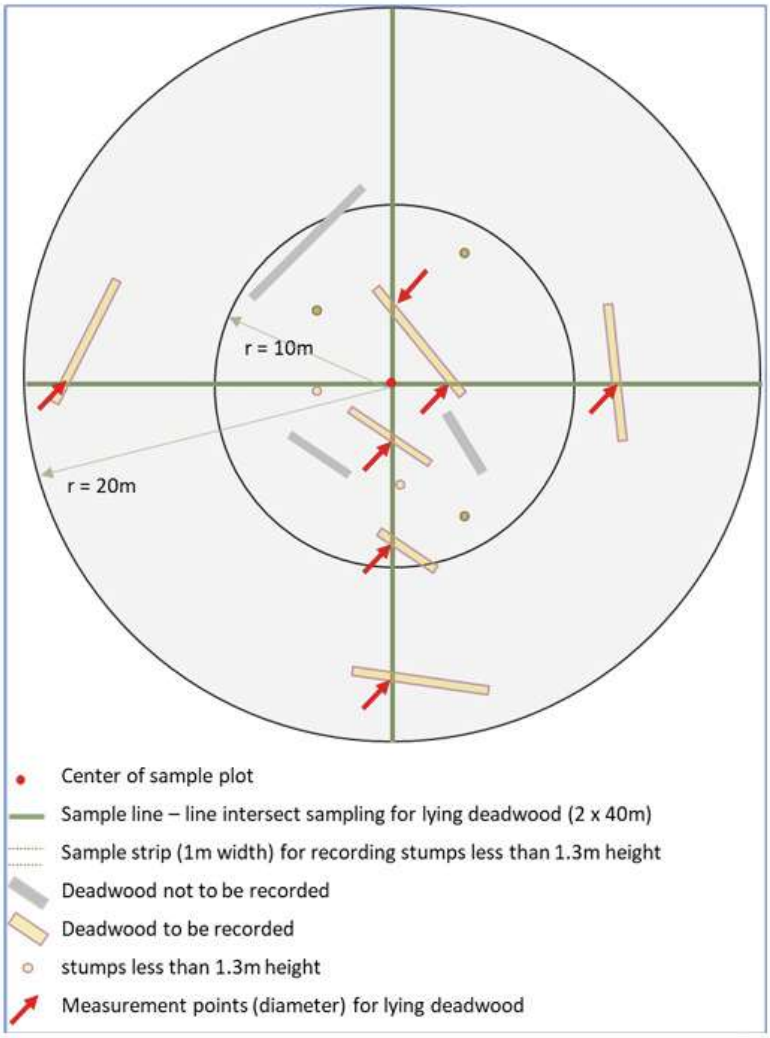

Figure 4.3: Visualisation of the Line Intersect Method (Kirchmeir et al., 2023)

The volume of lying deadwood was calculated using the Line Intersect Method as described by Wagner, 1968. The formula used for this calculation is:

$$V_{LG} = \frac{\pi^2 \sum_{l=1}^{L} d_L^2}{8L} \tag{4.1}$$

where V_{LG} represents the volume of lying deadwood m^3/m^2, d_L denotes the diameter of the cross-sectional area of each intersecting log, and L is the length of the transect measured in meters as a horizontal distance (Kirchmeir et al., 2023; Wagner, 1968).

4.1.4. Precise Manual Data Collection

Manual measurements of deadwood logs were carried out on the 7th and 8th October 2024. The plot center, pre-defined during earlier surveys, served as the reference point for all mea-

surements. A circular area with a radius of 12 meters was established around this center to delineate the boundary of the survey. All lying deadwood logs with a diameter greater than 10 cm were included in the survey. Thin branches, small logs, and logs that were heavily decomposed were excluded from the analysis. For logs that extended beyond the radius of 12 meters, only portions within the circular boundary were measured.
The diameter of each log was recorded using a diameter tape. Multiple measurements were taken along the length of each log, and the average of these measurements was calculated. Diameters were recorded to the nearest centimeter to ensure precision. The length of each log was measured using a 30-meter measuring tape, with lengths recorded to the nearest decimeter.
During the fieldwork, all measurements were noted in a sketch to provide a visual reference for the spatial distribution and individual characteristics of the logs. These sketches were later digitized for further processing and analysis.
The collected field data were processed to calculate the volume of each deadwood log. Using the average diameter ($d[m]$) and length ($l[m]$) measurements, the volume ($V[m^3]$) of each log was estimated by assuming a cylindrical shape:

$$V = \pi r^2 l \tag{4.2}$$

where $r = \frac{d}{2}$ represents the radius [m] of the log, derived from the recorded diameter. The assumption of a cylindrical shape provides a practical approximation of the wood volume, despite the irregularities of natural deadwood logs.
During the data processing, special care was taken to ensure that only the portions of logs within the survey boundary were included in the volume calculations. This was verified against the sketches and digitized data.
The results obtained through manual measurements serve as a baseline for comparison with other methods of estimating deadwood volume. In the results chapter, these values are directly compared with volumes derived from TLS, ULS, and the Line Intersect Method.

4.2. TLS Data Processing

4.2.1. Filtering of potential lying Deadwood stems

The coregistered TLS point cloud was first imported into OPALS (Pfeifer et al., 2014) to leverage its specialized modules for point cloud processing. A coordinate system was assigned to ensure compatibility for visual comparisons in GIS. Using the limit function, the point cloud was cropped to a smaller area around the center to streamline subsequent processing steps focused on the area of interest.
The basis of the entire computation relies on a normalized point cloud, achieved by calculating the Digital Terrain Model (DTM) using a hierarchical approach (Pfeifer and Mandlburger, 2018). For this computation, only the first echoes were used to ensure that the model accu-

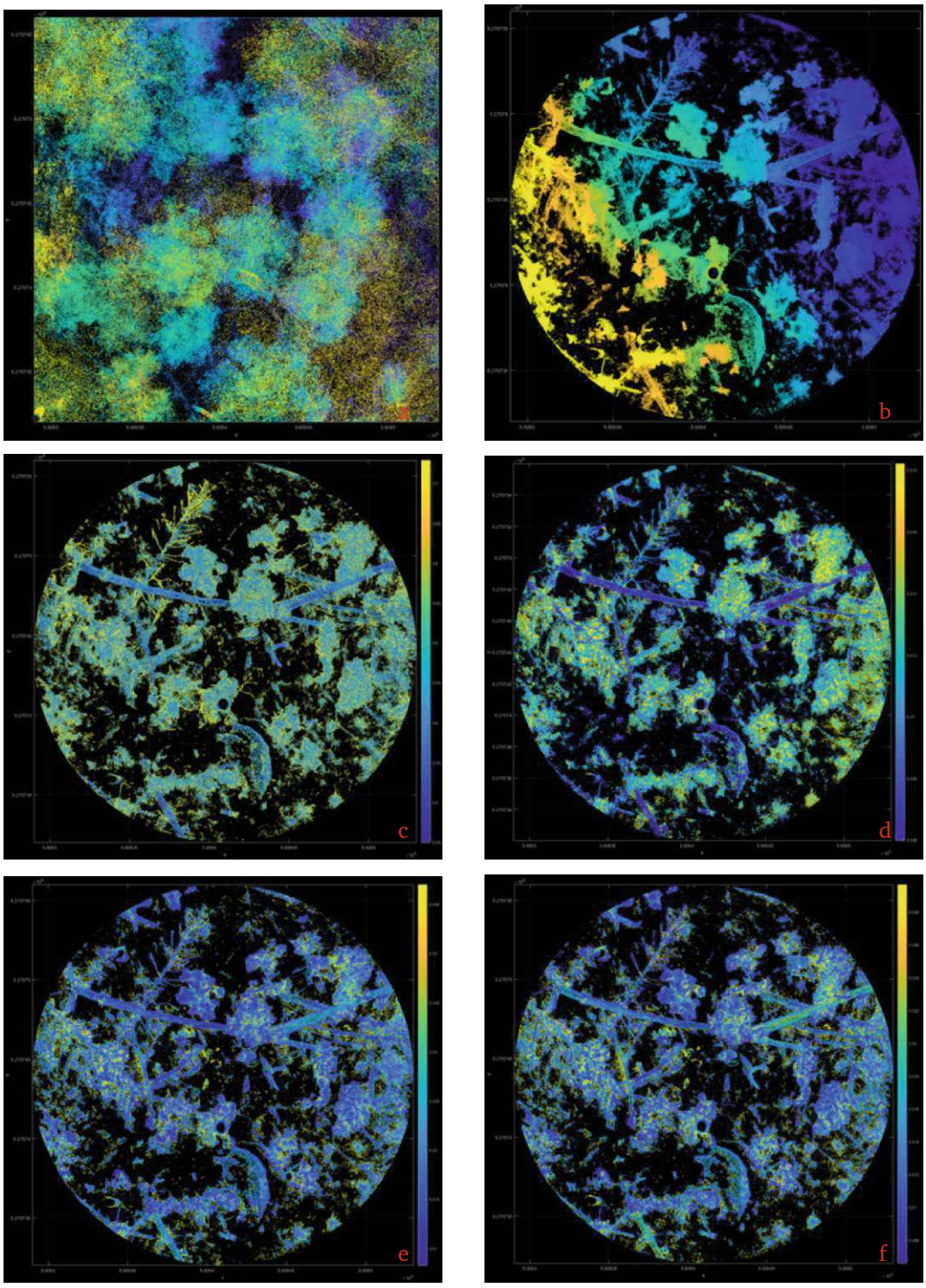

Figure 4.4: Visualisation of TLS Processing Steps. a) TLS PC; b) PC after normalization and cropping around the area of interest; c) calculated linearity of the PC; d) Sigma0 of Normal calculation; e) Eigenvalue 1; f) Eigenvalue 2

rately represents the ground surface, providing a reliable reference for future analysis steps. From the normalized point cloud, all points except those between 0.1 and 2.5 meters above

the ground were filtered out. The upper limit of 2.5 meters was chosen based on field observations, where no deadwood was found lying higher than this threshold. This filtering ensures that only relevant points that represent deadwood structures are retained for further analysis. The area of interest (AOI) was defined as a 12-meter radius around a specified center point. To remove points outside this AOI, the distance of each point from the center was calculated, and all points with a distance greater than 12 meters were filtered out (figure 4.4 b). The process starts by calculating the normal vectors for each point in the point cloud, providing essential information on the orientation of the surface. This is important to distinguish between the features of the terrain and the objects. To enhance precision, the calculation includes each point's 50 nearest neighbors. Additionally, both the largest eigenvalue of each local neighborhood's covariance matrix and the σ_0 value, which indicates the quality of the fit for the computed normals, are stored as metadata. These values are critical for subsequent characterizations of surface properties such as linearity and planarity. The search is carried out within a three-dimensional space, limited to a radius of 0.5 meters to balance computational efficiency with accuracy in detail. (Pfeifer et al., 2014)
Following this, a new attribute called "linearity" is added to the data set (Melzer and Briese, 2004), calculated based on the previously stored eigenvalues λ. This linearity attribute quantifies how much each point's local neighborhood aligns along a line, using the formula:

$$linearity = \sqrt{1 - \frac{\lambda_2}{\lambda_1}} \tag{4.3}$$

Here, the ratio of the two largest eigenvalues (representing the spread of neighboring points) indicates whether the points tend to form linear or edge-like structures. High $linearity$ values thus suggest alignment along a line, which can highlight the presence of linear features such as deadwood logs within the dataset. During visual inspection, branches exhibited the highest linearity values among objects in the dataset, while other complex features, such as foliage, demonstrated higher Normal Eigenvalues due to irregular structures and greater variance in point distribution. To isolate deadwood logs more effectively, a selective filtering approach was applied. The points were exported from the data set using specific criteria, regarding $Normalsigma0$ (Figure 4.4 d), $NormalEigenvalues$ (Figure 4.4 e, f) and $linearity$ (Figure 4.4 c) (Pfeifer et al., 2014).
Although this approach helped exclude many non-target features, additional points outside the intended deadwood logs remained in the point cloud. The $Normalsigma0$-threshold, crucial for identifying smoother surfaces by measuring the angular dispersion of normal vectors, aimed to retain only surfaces typical of deadwood logs or flat ground. However, certain points with similar values to deadwood characteristics were still present, indicating the need for further refinement. Combining this $NormalSigma0$ with lower $NormalEigenvalue$ thresholds improved the quality of the data set by filtering out high-complexity features, but additional steps are necessary to fully isolate deadwood logs in future processing stages.

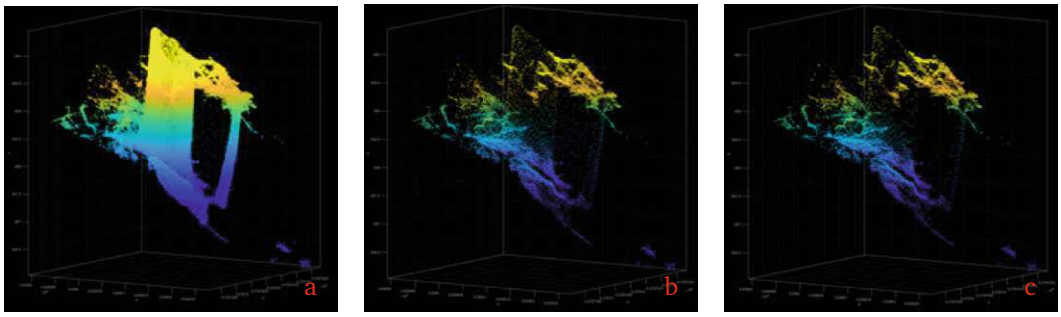

Figure 4.5: Standing Stem removal. a) TLS PC before removal steps; b) result after combining highest and lowest point of a 2 cm cell; c) result after removing all points with a higher distance than threshold

In the segmentation process, overlapping logs often merge into a single segment, which poses a challenge for accurate identification. To address the challenge of overlapping and intersecting logs, a quantile-based approach was applied. Specifically, the height quantiles 0.1 and 0.9 were used to create a vertical separation between the overlapping logs. For each 2-centimeter cell, only two points were retained: one in the 0.1 quantile and one at the 0.9 quantile. This method not only facilitated the separation of the overlapping logs, but also had the additional benefit of significantly reducing the point density on standing stems, making them easier to filter out during subsequent processing steps (Figure 4.5).
Next, the distance to the nearest neighbor is calculated for each point. This approach results in greater spacing on standing trees due to their reduced point density, facilitating easier differentiation. Points with distances exceeding a set threshold are then filtered out, further isolating deadwood logs and improving segmentation accuracy (Figure 4.5 (Pfeifer et al., 2014).

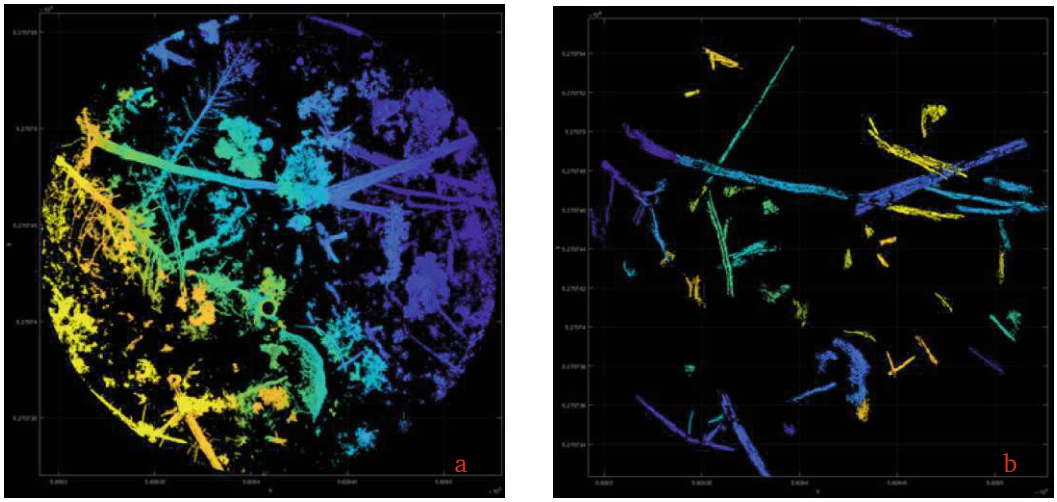

Figure 4.6: a) TLS PC after all filtering steps; b) Results after Segmentation

The segmentation module in OPALS is used to segment lying tree trunks. The *condclustering*

method (Pfeifer et al., 2014) is applied with a search radius of 0.2 meters and a minimum segment size of 300 points. To determine if TLS points lie on a common surface, the dot product between the $NormalEigenvector$ of each point and that of its neighboring points is calculated. This dot product measures the alignment between the normal vectors of neighboring points across the X, Y, and Z directions. By taking the absolute value of this scalar product, we obtain a measure of how closely aligned the two normal vectors are, regardless of direction. For points to be considered as lying on the same surface, this value must exceed the threshold cos(0.06). This threshold ensures that only points with closely aligned normal vectors are retained, effectively filtering out misaligned points and isolating those that lie on a common surface, thus facilitating accurate segmentation of individual lying tree trunks. Finally, all points that do not belong to any segment are removed (Figure 4.6 b). This step ensures that only points associated with well-defined segments, specifically the lying tree trunks, are retained for further analysis. (Pfeifer et al., 2014)

4.2.2. Determination of lying Deadwood Parameters

After segmenting potential deadwood trunks, further analysis is performed to extract relevant parameters, such as diameter, length, and volume. Additionally, if individual trunks were segmented separately, they are merged to ensure each deadwood trunk is represented as a single segment. This merging step refines the dataset, providing an accurate basis for assessing the characteristics and distribution of deadwood in the study area.

- Step 1. Load Input File

  The initial step involves processing the input file, which contains the point cloud data required for the analysis. This file is structured as a text file, with each row representing a single point in the point cloud. Each point is defined by its spatial coordinates (X, Y, Z) and the SegmentID, which groups points belonging to the same segment. The data is read into a structured format for further analysis, ensuring that all points and their associated attributes are accessible. The points are then grouped by their SegmentID, allowing the identification of distinct segments, such lying tree stem. This grouping facilitates the application of subsequent analysis methods, such as segmentation and parameter extraction.

- Step 2. Apply Initial RANSAC to Each Segment

  In this step, a RANSAC (Random Sample Consensus) regression (Fischler and Bolles, 1981) is applied to each segment in the point cloud to establish an initial polynomial model representing the shape of the tree stem sections. The primary goal of this step is to create a robust preliminary fit for each segment without filtering based on model quality at this stage. The points in the point cloud are grouped by their `SegmentID`, allowing the analysis of each segment independently. The x and y coordinates of the

points within each segment are extracted, enabling the representation of the segment in a two-dimensional space. To account for the characteristic curvature of tree stems, a polynomial transformation is applied to the data. A quadratic polynomial is typically used, which enables a parabolic fit. The polynomial model for a segment is expressed as:

$$y = a_0 + a_1 x + a_2 x^2 \tag{4.4}$$

where a_0, a_1, and a_2 are the polynomial coefficients. These coefficients are determined by fitting the transformed data to a linear regression model, ensuring the best-fit curve for the segment points. To streamline this process, the polynomial transformation and regression fitting are combined into a single workflow.

RANSAC regression is then employed to refine the polynomial model. This approach minimizes the influence of outliers, such as stray points or small branches, by iteratively sampling subsets of points, fitting models, and selecting the one that best captures the main structure of the segment. This ensures that the polynomial model predominantly represents the primary stem geometry, while deviations caused by noise are ignored (Fischler and Bolles, 1981).

Although a 3D polyline would provide a more precise representation for complete cylinders, this is not feasible in the current dataset. Prior filtering steps often result in missing portions of cylindrical surfaces, particularly for logs lying on the ground, where the lower part of the cylinder is frequently absent. Consequently, the fitted line aligns with the visible edge rather than the central axis, leading to potential inaccuracies in diameter estimates. Therefore, a 2D approach is adopted to approximate the geometry, balancing simplicity and robustness.

Following the RANSAC fitting, essential details for each segment are recorded, including the polynomial model and the minimum and maximum x values (x_{min} and x_{max}). Additionally, the predicted y-coordinates at these endpoints, $\hat{y}_{\text{min}}$ and $\hat{y}_{\text{max}}$, are calculated using the fitted polynomial model:

$$\hat{y}_{\text{min}} = a_0 + a_1 x_{\text{min}} + a_2 x_{\text{min}}^2 \tag{4.5}$$

$$\hat{y}_{\text{max}} = a_0 + a_1 x_{\text{max}} + a_2 x_{\text{max}}^2 \tag{4.6}$$

These values provide an initial geometric representation of each segment and serve as the foundation for further processing. By the end of this step, each segment is characterized by an independent polynomial model, forming the basis for subsequent segment merging and refinement.

- Step 3. Segment Merging Based on Proximity, Orientation, and Height Difference

In this step, individual segments are merged to ensure that fragmented parts of the same tree stem are combined into a single segment. The merging process is guided by three criteria: spatial proximity, alignment in orientation, and similarity in height. These checks ensure that only segments likely representing the same tree stem are merged, avoiding erroneous combinations of overlapping or stacked segments.

Proximity Check

To determine spatial closeness, the distance between the endpoint of one segment and the start point of another is calculated using the Euclidean distance:

$$d = \sqrt{(x_{\text{end1}} - x_{\text{start2}})^2 + (y_{\text{end1}} - y_{\text{start2}})^2} \tag{4.7}$$

The coordinates $(x_{\text{end1}}, y_{\text{end1}})$ represent the endpoint of the first segment, while $(x_{\text{start2}}, y_{\text{start2}})$ refer to the start point of the second segment. These points are used to calculate the proximity between segments, which is a critical step in determining whether they should be merged.

Segments are considered close enough for merging if d is less than a predefined threshold ($d_{\text{threshold}}$).

Orientation Check

Alignment between segments is evaluated by comparing their tangent directions at the endpoints. The tangent vector for each segment is derived from the polynomial fit. The angle θ between the tangent vectors of two segments is calculated using the dot product:

$$\cos(\theta) = \frac{\vec{v_1} \cdot \vec{v_2}}{|\vec{v_1}||\vec{v_2}|} \tag{4.8}$$

$\vec{v_1} = (1, f_1'(x_{\text{end1}}))$: Tangent vector of the first segment. $\vec{v_2} = (1, f_2'(x_{\text{start2}}))$: Tangent vector of the second segment.

Segments are aligned closely enough for merging if the angle θ is below a predefined threshold.

Height Difference Check

The vertical alignment of segments is assessed by calculating the height difference (Δz) between the endpoint of the first segment and the start point of the second:

$$\Delta z = |z_{\text{end1}} - z_{\text{start2}}| \tag{4.9}$$

The height of the endpoint of the first segment is denoted by z_{end1}, while the height of the start point of the second segment is represented as z_{start2}. Segments are considered for merging if the height difference, Δz, is below a predefined threshold, $z_{\text{threshold}}$.

Merging Procedure

If two segments meet all three criteria, their points are combined, and the bounding coordinates $(x_{\min}, x_{\max}, z_{\min}, z_{\max})$ are updated to reflect the extent of the merged segment. This process is iteratively applied to all segment pairs, ensuring that the dataset accurately represents unified tree stems while maintaining segmentation integrity.

This step effectively reduces fragmentation and enhances the continuity of tree stem data, providing a solid foundation for further parameter extraction and analysis.

- Step 4. Reapply Ransac to Merged Segments and Quality Assurance

  In this step, RANSAC regression is reapplied to each segment resulting from the merging process to refine the polynomial model. This ensures that the updated model accurately represents the complete structure of each newly combined tree stem section, which may differ from the initial models due to the integration of multiple segments.

  For each merged segment, all associated points are retrieved, including those combined during the merging process. These points are used to refit a polynomial model, applying the same procedure as in Step 2. The polynomial transformation is performed, and a RANSAC regression pipeline is employed to robustly fit the model, minimizing the influence of outliers and ensuring the best possible representation of the segment's overall structure. This reapplication of RANSAC ensures that the polynomial accurately reflects the geometry of the entire segment, even after merging.

  Quality Assurance with R^2 Evaluation

  Following the RANSAC fitting, a quality assurance step is conducted to evaluate the reliability of the polynomial model for each segment. The coefficient of determination (R^2) (Cheng et al., 2014) is calculated, which measures how well the polynomial model explains the variance in the segment's y-coordinates. The formula for R^2 is:

$$R^2 = 1 - \frac{\sum_{i=1}^{n}(y_i - \hat{y}_i)^2}{\sum_{i=1}^{n}(y_i - \bar{y})^2} \tag{4.10}$$

  In this formula, y_i represents the observed y-coordinate of each point, $\hat{y}_i$ denotes the predicted y-coordinate from the polynomial model, and $\bar{y}$ is the mean of all observed y-coordinates in the segment. The total number of points in the segment is denoted as n. An R^2 value close to 1 indicates that the model fits well and explains most of the variance in the data, while lower values suggest a poorer fit. Segments with an R^2 value below a predefined threshold are excluded from further analysis, as they may not adequately represent the expected structure of a tree stem.

  By reapplying RANSAC and implementing a quality assurance step, this process ensures that only well-represented segments proceed to subsequent analysis stages, improving the accuracy and reliability of the results.

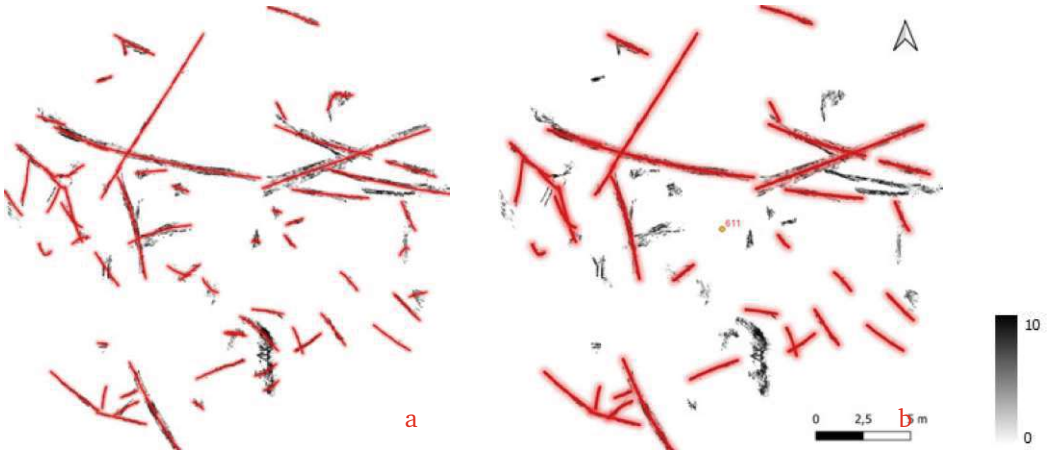

Figure 4.7: a) Results after the first iteration of poly line fitting with Ransac; b) Results after the second iteration in front of a raster point density map.

- Step 5. Calculate Segment Parameters (Diameter, Length, and Volume)

  In this step, the geometric parameters **diameter**, **length**, and **volume** are calculated for each segment that passed the quality assurance in Step 4. These parameters provide a detailed representation of the structure of each CWD, based on the final polynomial model fitted to the merged segments.

  Diameter Calculation

  The diameter of each segment is estimated by analysing the residuals of the polynomial fit. Residuals represent the difference between the observed y-coordinates and the corresponding y-coordinates predicted by the polynomial model:

$$\text{Residual}_i = y_i - \hat{y}_i \tag{4.11}$$

  where y_i is the observed y-coordinate, and $\hat{y}_i$ is the predicted value from the polynomial model.

  The diameter is calculated based on the spread of these residuals by computing specific quantiles, such as the 0.15 and 0.85 quantiles. The lower and upper quantiles, denoted as q_{lower} and q_{upper}, respectively, are used to approximate the diameter d:

$$\text{d} = |q_{\text{upper}} - q_{\text{lower}}| \tag{4.12}$$

  This approach captures the vertical spread of points around the polynomial curve, providing a reliable estimate of the segment's diameter.

  Length Calculation

  The length of each segment is determined using the arc length of the polynomial curve fitted to the segment, adjusted for vertical displacement in the z-coordinates. The

arc length in the x-y plane 2D-length is calculated by integrating the polynomial's derivative over the range of x-coordinates:

$$\text{2D-Length} = \int_{x_{\min}}^{x_{\max}} \sqrt{1 + \left(\frac{dy}{dx}\right)^2}\, dx \tag{4.13}$$

The derivative $\frac{dy}{dx}$ is derived from the polynomial model:

$$\frac{dy}{dx} = a_1 + 2a_2 x \tag{4.14}$$

To account for the vertical offset, the difference in z-coordinates between the endpoints, denoted as $\Delta z = z_{\max} - z_{\min}$, is included. The actual segment length, reflecting the true 3D distance, is then calculated using the Pythagorean theorem:

$$\text{Actual Length} = \sqrt{(\text{2D-Length})^2 + (\Delta z)^2} \tag{4.15}$$

Volume Calculation

Once the diameter and length are determined, the volume of each segment is approximated by assuming a cylindrical shape. The formula for the volume V is given as:

$$V = \pi \left(\frac{d}{2}\right)^2 \times \text{Actual Length} \tag{4.16}$$

This calculation assumes a circular cross-section, which is a reasonable approximation for tree stems. The resulting volume provides an estimate of the total size of the segment, offering valuable insights for ecological and forest applications. By calculating the diameter, length, and volume for each segment, this step provides a comprehensive quantitative description of the tree stems. These parameters are crucial for assessing the structural characteristics of deadwood, enabling further analysis of ecological processes and resource quantification.

- Step 6. Save Results and Export Data

  In this final step, the processed data is organized and exported for further analyses and visualisation. The parameters calculated for each segment are saved in multiple formats to support various research workflows and spatial applications. A CSV-file is generated to store key metrics for each segment, including its unique identifier, calculated length, diameter, volume, and mean residual. This tabular format ensures compatibility with a wide range of statistical and analytical tools, enabling efficient quantitative evaluation of the data. Furthermore, an extended point cloud file is exported, preserving the original x, y, and z coordinates of each point alongside the

corresponding segment parameters. This extended format allows for advanced spatial analyses and integration into point cloud processing software, providing researchers with a detailed dataset for further exploration. To enable geospatial visualisation and integration into Geographic Information System (GIS) software, each segment is also saved as a Shapefile. The Shapefile format represents each segment as a polyline derived from the fitted polynomial model and includes attributes such as segment ID, length, diameter, and volume. This georeferenced representation facilitates the visualisation of individual tree stems and their spatial relationships within the study area. The availability of these outputs in multiple formats (CSV, extended point cloud, and Shapefile) ensures flexibility in data usage. The exported datasets not only support detailed quantitative analyses but also provide a robust foundation for spatially informed research and visualisation. These outputs are crucial for integrating the findings into broader ecological studies and forest management practices, highlighting the adaptability of the developed methodology to diverse research contexts.

- Step 7. Outlier Detection

  To ensure the accuracy and reliability of the results, an outlier detection step is applied based on the diameter of the detected logs. Empirical observations in the study areas revealed that no tree logs exceed a diameter of 65 cm. Consequently, a maximum diameter threshold of 68 cm is established. Any segment with a calculated diameter above this value is discarded as an outlier.

  This step is crucial to prevent overestimated log dimensions from distorting the deadwood volume estimation. By excluding implausibly large segments, the analysis focuses on logs that align with realistic conditions observed in the field. While this criterion reduces the number of segments included in the final analysis, it minimizes the risk of errors introduced by outliers, ensuring that the results remain both accurate and reliable.

4.3. Data Validation

To validate the results, the manual in situ measurements serve as the reference dataset. The newly developed TLS approach calculates the parameters of lying deadwood for each individual log. Consequently, these results are compared against the corresponding manually measured data on a log-by-log basis by calculating the mean deviation and RMSE. This allows for an evaluation of the accuracy of the TLS-derived parameters, including length, diameter, and volume.

$$\text{RMSE} = \sqrt{\frac{\sum_{i=1}^{n}(\hat{y}_i - y_i)^2}{n}} \tag{4.17}$$

Here, $\hat{y}_i$ represents the predicted value (e.g., parameters estimated by the TLS method), y_i

represents the true value (e.g., manual measurements), and n denotes the total number of stems. The difference $(\hat{y}_i - y_i)$ measures the deviation between the predicted and true value, while $(\hat{y}_i - y_i)^2$ computes the squared deviation to treat both positive and negative errors equally.

In contrast, the described ULS-based method and the Line Intersect Method provide the total deadwood volume for the entire study area, rather than the parameters for individual logs. Therefore, the results of these methods are compared at the aggregate volume level. This comparison highlights the differences in the results between the methods and helps identify their respective strengths and limitations in various forest conditions.

The validation process further illustrates how specific challenges in the field, such as overlapping logs, dense vegetation, or fragmented deadwood, can influence the performance of each method. This analysis not only provides information on the reliability of the methods, but also offers guidance on their applicability under different forest environments.

5. Results

In this chapter, we focus on the results obtained for the three study plots: 610, 611, and D3. The analysis is divided into two parts. First, we examine the TLS-based method, which determines the parameters of individual logs, such as diameter, length, and volume, providing detailed insight into its performance and accuracy. Subsequently, we evaluate the methods used to estimate the total deadwood volume for all plots, allowing a comparative assessment of their effectiveness and reliability in capturing the overall biomass.

5.1. TLS Per Log Results

This section examines the results of the TLS method compared to manual measurements. For each log, the detection success of the TLS method is evaluated and derived parameters such as diameter, length, and volume are compared to the manual measurements. Manual measurements are treated as reference values that serve as a benchmark to assess the accuracy of the TLS-derived parameters. This approach ensures a systematic evaluation of the TLS method's ability to replicate manually measured results.

Segments identified by the TLS approach that do not correspond to any logs recorded in the manual measurements are excluded from this analysis. These segments will be addressed in subsequent sections.

Examining the results of Plot 611 (Table 5.1), 84% of the deadwood logs manually recorded in the field were successfully detected using the TLS method. This detection rate demonstrates a high level of agreement between the TLS-derived results and the manual measurements, highlighting the method's reliability in identifying deadwood logs within this plot.

In plot 611, length, diameter and volume were determined for each detected log, with results showing that the majority of the parameters were measured with a high level of precision. However, two logs, identified by segment IDs 3 and 19, were split into separate parts and recorded as distinct segments in the data set (Table 5.1).

A log, identified as Segment 18 and highlighted in gray in the results Table 5.1, was classified as an outlier. Its diameter exceeds the maximum threshold established in the Methodology chapter, confirming it as inconsistent with the expected parameters. This exclusion ensures that the analysis remains accurate and unaffected by implausible measurements.

Table 5.4 summarizes the deviations and variability of the parameters. In plot 611 the mean deviation of the log length is -0.34 m, with a RMSE of 0.96 m. For diameter, the mean deviation is 3 cm, with a RMSE of 12 cm. For volume, the mean deviation is 0.05 m^3, with a RMSE of 0.376 m^3. The mean deviation of the three parameters shows that the length is underestimated, while the diameter and length are slightly overestimated. Table 5.4 also shows the number of logs that were detected by the TLS method and participated in the validation process.

Table 5.1: Comparison of Results Between Manually Measured and TLS-Derived Logs by Segment ID, Plot 611

Stem ID	**TLS**			**Manual**		
	l (m)	d (cm)	V (m^3)	l (m)	d (cm)	V (m^3)
1	2,7	0,34	0,245	2,1	0,36	0,214
2	4,1	0,41	0,542	4,5	0,51	0,919
3	9,45	0,35	0,926	16,3	0,4	2,048
3/2	5,39	0,24	0,24			
4	0,26	0,28	0,286	10,8	0,12	0,122
5	8,65	0,53	1,88	8,5	0,45	1,352
6	11,5	0,56	2,763	11,3	0,53	2,449
7	3,19	0,32	0,262	2,7	0,34	0,245
8				6,5	0,25	0,319
9				4,7	0,21	0,163
10	1,7	0,59	0,45	1,8	0,20	0,057
11				1,7	0,24	0,077
12	1,97	0,18	0,051	2	0,14	0,031
13	3,1	0,14	0,053	3,1	0,18	0,079
14	5,9	0,65	1,963	5,8	0,51	1,185
15	2,8	0,13	0,036	2,7	0,15	0,048
16	1,7	0,28	0,105	1,9	0,26	0,101
17	3,6	0,16	0,074	3,4	0,18	0,087
18	5,7	1,24	6,080	5,5	0,12	0,062
19	3,1	0,34	0,287	8,1	0,31	0,611
19/2	2,18	0,3	0,150			

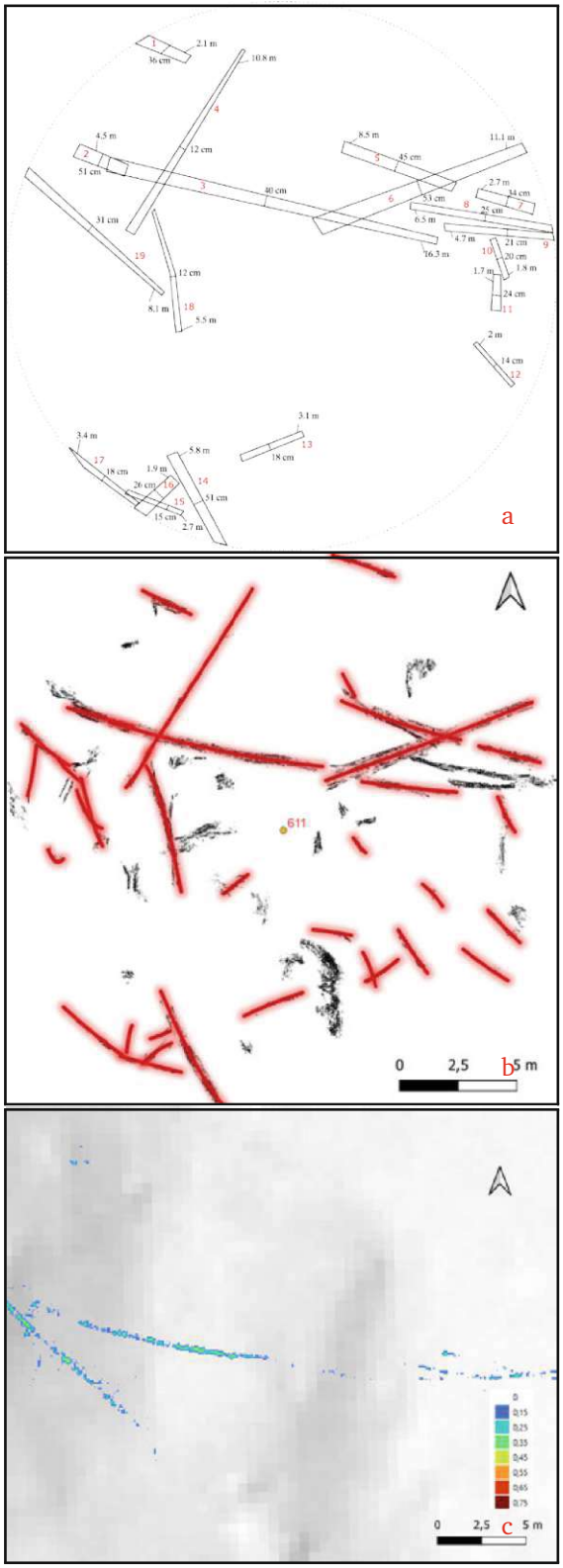

Figure 5.1: Results Plot 611; a) Manual Measurements of lying deadwood with SegmentID (red), mean diameter and length; b) TLS-Method results, showing polyline fit above a point count raster map; c) ULS Method Results: Voxel-Based Approach and Diameter Mapping of Deadwood

Figure 5.1 shows the results of three different methods for detecting deadwood logs. Subfigure (a) shows the manually measured logs, while subfigures (b) and (c) display the logs detected using the TLS method and the ULS method. Figure 5.1c is colored by the determined log diameter.

In Figure 5.1b, the red lines represent the shapefiles of the fitted polylines for each segment, providing a geometric outline of the detected logs. Figure 5.1b includes the rasterized visualization of the point count.

The analysis shows that the TLS method (Figure 5.1b) detects a larger number of deadwood logs compared to manual measurements. However, it also identifies additional fragments that were not classified as deadwood logs during field surveys. In some cases, branches were incorrectly detected as logs. The ULS-based method (Figure 5.1c) detected 26% of the deadwood stems recorded during manual measurements.

Table 5.2: Comparison of Results Between Manually Measured and TLS-Derived Logs by Segment ID, Plot 610

Stem ID	**TLS**			**Manual**		
	l (m)	d (cm)	V (m^3)	l (m)	d (cm)	V (m^3)
1				8,2	0,26	0,435
2				5,2	0,24	0,235
3	6,9	0,67	2,489	4,3	0,3	0,304
4				4,8	0,27	0,275
5	2,9	0,42	0,405	5,6	0,31	0,423
6				8,5	0,38	0,964
7	3,2	0,27	0,188	3	0,31	0,226
8	2,9	0,5	0,727	11,5	0,32	0,925
9				7	0,3	0,495
10				8,5	0,38	0,964
11	4	0,95	2,898	5,9	0,3	0,417
12				3,5	0,2	0,110
13				3,3	0,28	0,203
14	2,9	0,28	0,187	3,3	0,24	0,149
15				5	0,22	0,190
16	1,7	0,47	0,394	5,2	0,28	0,320
17	5,9	0,65	1,978	6	0,26	0,319
18	1,9	0,21	0,070	1,5	0,23	0,062
19				3	0,28	0,185
20				1,5	0,11	0,014
21				3,8	0,14	0,058

The results of plot 610 present a different picture compared to the previous analyzes (Figure 5.2). A significantly smaller proportion of deadwood logs was detected, with only 48% of the logs identified during manual measurements being captured.

A closer examination of the deadwood parameters reveals notable deviations between the

detected values and the manually measured values. In particular, the differences in diameter and volume are considerably larger (Table 5.4). The analysis shows an average length difference of -1.5 meters between the TLS and manual measurements, with a RMSE of 3.5 meters. For the diameter, an average deviation of 15 cm with a RMSE of 22 cm was observed, resulting in a mean volume difference of 0.46 m^3. The RMSE for volume amounts to 0.973 m^3. Furthermore, one outlier was identified: the log with ID 11. This log exhibits particularly large deviations in its measured parameters.

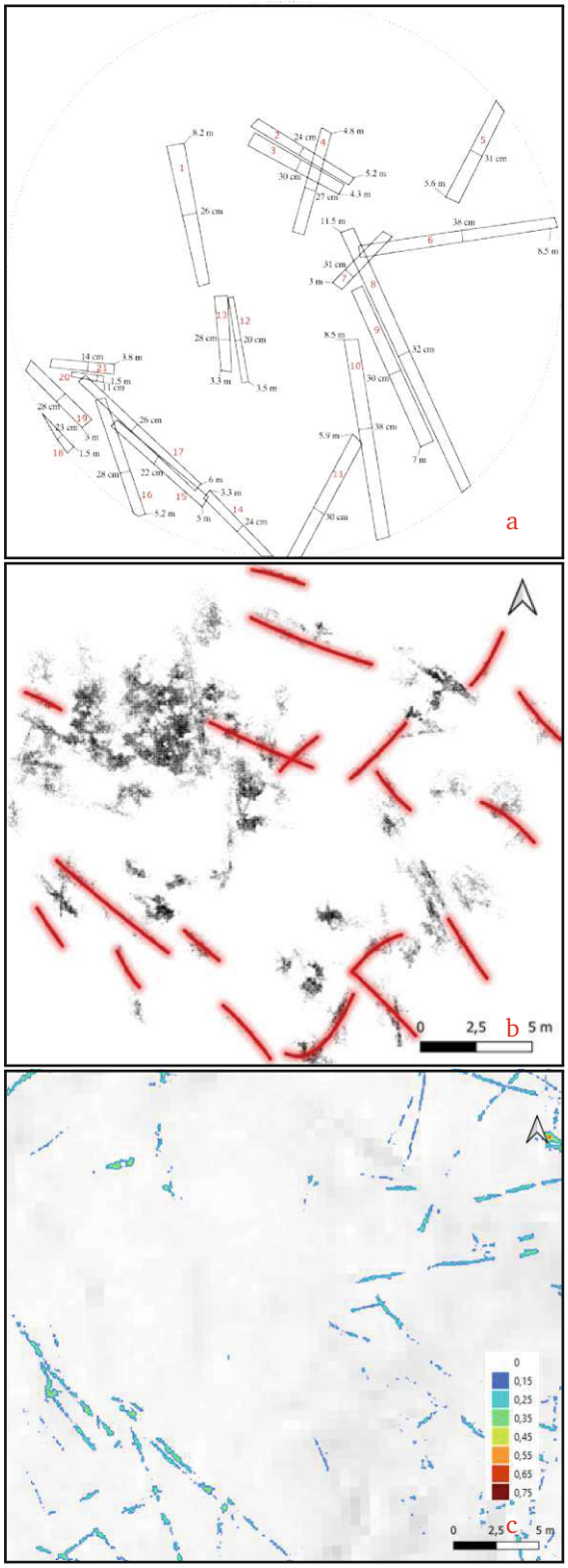

Figure 5.2: Results Plot 610; a) Manual Measurements of lying deadwood with SegmentID (red), mean diameter and length; b) TLS-Method results, showing polyline fit above a point count raster map; c) ULS Method Results: Voxel-Based Approach and Diameter Mapping of Deadwood

Figure 5.2 presents the results of the manual method, the TLS method and the ULS method. The results indicate that the TLS method (Figure 5.2b) performed inconsistently in detecting deadwood logs in several areas. Similarly, the ULS method (Figure 5.2c) detected a significantly smaller number of deadwood logs compared to manual measurements. From a visual interpretation perspective, the ULS method identified 43% of the deadwood logs recorded during manual measurements. Moreover, both methods did not detect the entire length of many logs; instead, they captured only portions of the logs identified. The reason for these differences in the results compared to plot 611 is given in the next chapters.

Table 5.3: Comparison of Results Between Manually Measured and TLS-Derived Logs by Segment ID, Plot D3

Stem ID	**TLS**			**Manual**		
	l (m)	d (cm)	V (m^3)	l (m)	d (cm)	V (m^3)
1				1,9	0,45	0,302
2	2	0,22	0,079	8,3	0,15	0,147
3	5,9	0,58	1,582	7,9	0,6	2,234
4	3,1	0,34	0,285	9,3	0,21	0,322
5	4,1	0,39	0,493	10,3	0,45	1,638
5/2	2,5	0,31	0,189			
5/3	2,5	0,35	0,243			
5/4	3,1	0,31	0,240			
5/5	3,1	0,28	0,189			
6				6,8	0,12	0,077
7	5,4	1,12	5,310	5,5	0,5	1,080
8	3,4	0,67	1,210	2,2	0,3	0,156
9				3	0,1	0,024

The TLS results of plot D3, the long-term experimental plot, show that 56% of the deadwood logs were successfully detected. However, a closer analysis reveals several noteworthy findings and limitations in the detection process.

First, deviations between the detected and manually measured parameters were observed. The detected log lengths showed an average deviation of −1.7 m, with a RMSE of 4.7 m. For log diameters, the mean deviation was 9 cm, accompanied by a RMSE of 19 cm. The log volumes exhibited an average deviation of 0 m^3, with a RMSE of 0.57 m^3. It is important to note that the mean deviation (not the mean absolute deviation) is used to assess whether each parameter is overestimated or underestimated. In plot D3, the volume parameter shows deviations in both directions that largely balance each other out, resulting in a relatively small mean deviation (Table 5.3). These findings emphasize the variability in the accuracy of the parameters for the detected logs.

Two specific issues in the detection process require attention. The log with ID 7 was identified as an outlier due to significant deviations in its detected parameters. To ensure the reliability

of the analysis, this log was excluded from all subsequent calculations. Furthermore, the log with ID 5 was fragmented into five separate parts during the detection process. This segmentation likely affected the accuracy of the parameters for this log, demonstrating a limitation in the detection method's ability to accurately represent entire logs.

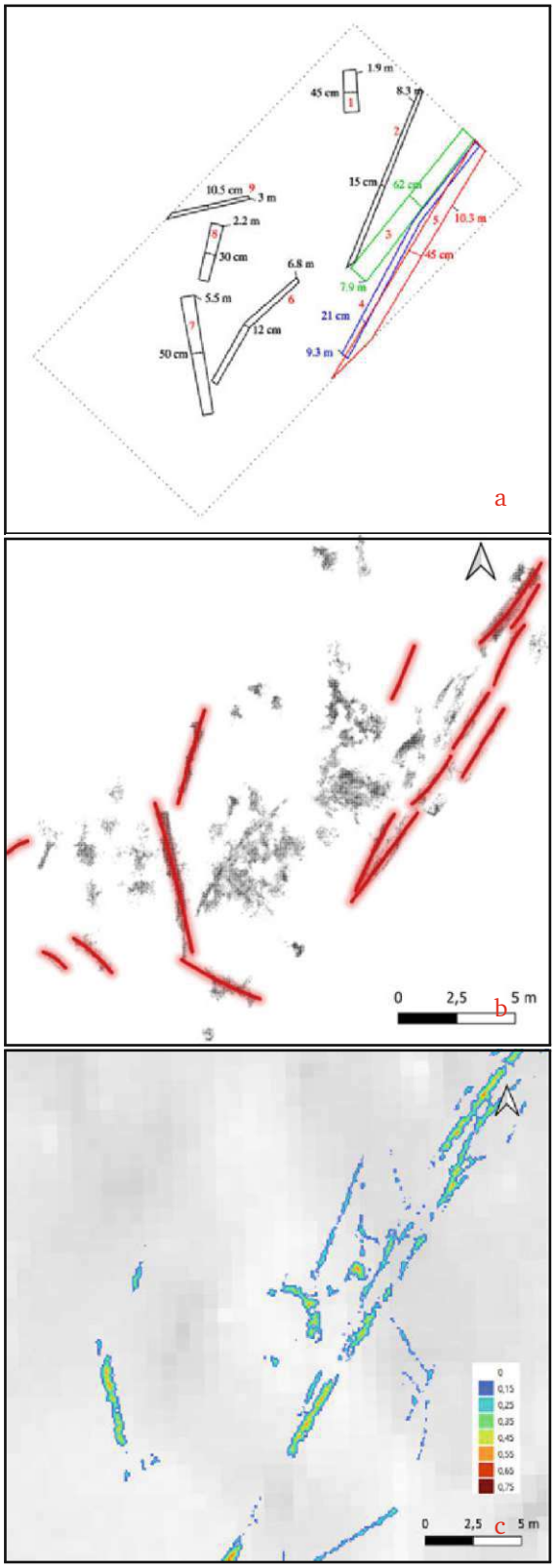

Figure 5.3: Results Plot D3; a) Manual Measurements of lying deadwood with SegmentID (red), mean diameter and length; b) TLS-Method results, showing polyline fit above a point count raster map; c) ULS Method Results: Voxel-Based Approach and Diameter Mapping of Deadwood

Next, we take a closer look at the results presented in Figure 5.3. It is evident that the large log shown in Figure 5.3a, with a diameter of 62 cm and a length of 7.9 m, is barely detected by both the TLS and ULS methods. However, both TLS and ULS successfully detected the smaller log with ID 5.
According to this evaluation method, the ULS approach detected 67% of the logs. However, some discrepancies are noticeable. For example, the log with ID 2 appears significantly shorter in the detection results compared to manual measurements. These findings highlight the limitations of automated detection methods, particularly in accurately capturing the dimensions of certain logs, as seen with ID 2 and the large log in Figure 5.3a.

Table 5.4: Deviations of the TLS-derived parameters from the in situ reference data for the plots, including the correctly identified logs and the number of correctly identified logs compared to the true total number of logs.

Plot	**611**	**610**	**D3**	**Total**
MeanDev Length [m]	-0,3	-1,5	-1,7	-0,9
RMSE Length [m]	0,9	3,5	4,7	2,8
MeanDev Diameter [m]	0,03	0,15	0,09	0,08
RMSE Diameter [m]	0,12	0,22	0,19	0,16
MeanDev Volume [m^3]	0,051	0,464	0,003	0,16
RMSE Volume [m^3]	0,373	0,973	0,570	0,636
Correctly identified logs	15/19	8/19	5/9	28/47

In conclusion, when considering the results of the combined three graphs (Table 5.4), the analysis revealed that the log length had a mean deviation of −0.9 m with a RMSE of 2.8 m. Similarly, the log diameter showed a mean deviation of 0.08 m and a RMSE of 0.16 m. For the log volume, the mean deviation was 0.16 m^3, accompanied by a RMSE of 0.635 m^3. This indicates that, while the length tends to be underestimated, the overestimation of the diameter results in an overall overestimation of the volume.

5.2. Results of Deadwood Volume Estimates Across Methods

Next, we examine the results of the different methods: manual measurements, Line Intersect, ULS, and TLS (Table 5.5). The results for Line Intersect and ULS were created using the methods from Kirchmeir et al., 2023.
The analysis reveals significant differences in the performance of the methods tested to estimate the volume of dead wood across the plots.
For the Line Intersect method, the results indicate that it captures approximately 45% of the volume manually measured in plot 611. In plot 610, the deviation is slightly smaller, with the method estimating about 74% of the manually determined volume, corresponding to a shortfall of 1.6 m^3. In plot D3, the Line Intersect method achieves a relatively accurate result, recording approximately 94% of the manual measurement, with only a minimal deviation

Table 5.5: Total lying deadwood volume in m^3 in Plot 611, 610 and D3 across the different Methods Manual, Line Intersect, ULS and TLS

Plot	**Manual [m^3]**	**Line Intersect [m^3]**	**ULS [m^3]**	**TLS [m^3]**
611	10,168	4,655	0,676	12,624
610	7,274	4,808	1,851	6,432
D3	5,979	5,650	2,826	4,317

of 0.3 m^3. In total, the Line Intersect method identifies 64% of the lying deadwood volume in the three plots.

However, the ULS approach significantly underestimates the volume of deadwood in all plots. In plot 611, it detects only a small fraction of the total biomass, accounting for just 7% of the manually measured volume. Performance improves slightly in plot 610, where 29% of the volume is detected. The best result is achieved in the plot D3, with the ULS method capturing 47% of the total volume. However, it is evident that this method consistently underestimates the lying deadwood volume across all plots. In total, the ULS approach identifies 22% of the lying deadwood volume in the three plots.

As the Figure 5.1 shows, the TLS method not only detected the logs identified during manual field measurements, but also classified additional fragments as deadwood. These fragments are included in the results as part of the estimated deadwood biomass.

As shown in Table 5.5, the TLS method estimated slightly more deadwood biomass in plot 611, with an additional 2.5 m^3 (124%) compared to manual measurements. In contrast, for plot 610, where the detection performed less effectively, the TLS method estimated 0.8 m^3 less deadwood biomass than manual measurements (88%). This is still a high value; however, when examining the visual results in Figure 5.1, we must assume that this is more likely due to coincidence. In plot D3, the TLS method estimated 77% compared to manually recorded data. In total, the TLS approach identifies 99% of the lying deadwood volume in the three plots. Additionally, this result requires further examination in the discussion section.

6. Discussion

In the discussion, we examine specific scenarios in natural environments to identify the reasons why the TLS method performed better or worse in certain areas. This analysis allows us to evaluate the strengths and weaknesses of the developed method. By understanding these strengths and weaknesses, we can explore ways to refine and optimize the method further in the future. Alternatively, we can determine under which conditions the TLS method is most suitable and when its application may be less effective. This will help to decide whether and when to rely on this method for practical use. Furthermore, we discuss the advantages and disadvantages of the different methods. ULS-based, TLS-based, manual measurements and the Line Intersect method. In addition, we evaluate the reliability of each method to provide a complete understanding of their performance and applicability under various conditions.

6.1. TLS-approach overall and Log-by-Log Discussion

Polewski et al., 2017 and Yrttimaa et al., 2019 report in their studies on the detection of lying deadwood using TLS that they achieved a detection rate of 70-80% in forests with moderate to dense vegetation. This is comparable to the 84% achieved in plot 611 in this study. However, the detection rate in Plot 610 was significantly lower at 48%, probably due to the denser vegetation and more heavily overgrown deadwood logs in this plot. Plot D3 achieved a detection rate of 67%, which is also below the results reported by Polewski et al., 2017. Combining the data from all three plots, the TLS method derived 99% of the lying deadwood volume. However, this result should be interpreted with caution, as it is the result of an overestimation in plot 611 being perfectly balanced by underestimations in plots 610 and D3.

The RMSE of the measured parameters also shows similarities with those in the literature. In this study, for example, the length RMSE was 2.82 m for the plot 611, while Yrttimaa et al., 2019 reports a RMSE of approximately 7.2 m. The diameter measurements also show consistency: the RMSE in this study was 0.16 m, comparable to Yrttimaa et al., 2019 (0.06 m) and also aligning with the results of Polewski et al., 2017. The RMSE of volume per stem for plot 611 (0.363 m^3) also aligns with Yrttimaa et al., 2019 (RMSE volume 0.305 m^3). These consistencies highlight the robustness of the TLS approach used in this study, especially in areas with moderate conditions, such as plot 611. However, for the other plots, the RMSE are less consistent with the literature. For plot 610, the RMSE for length was 3.55 m, and for plot D3, it was 4.66 m, both appear smaller compared to findings in previous research, although it is important to note that the overall stem length is shorter than in these other studies. Similarly, the RMSE for diameter were 0.21 m (plot 610) and 0.18 m (plot D3), indicating greater variability in these measurements compared to plot 611. This results in bigger RMSE for volume (0.973 m^3 plot 610 and 0.569 m^3 plot D3). To better understand these discrepancies, we will examine each plot in detail to identify the specific factors that

contribute to these differences.

We begin with plot 611, where the detection of deadwood using the TLS method performed the best. As shown in Figure 6.1, the plot is located on a slope, with fallen trees lying along the slope. In Figure 6.1b, we can observe a large log suspended in the air, lying across another large log, as well as three additional logs positioned on the ground in the lower right corner. Comparing these observations with the results in Figure 5.1a, which displays the outcomes of the manual measurements and the TLS method, we see that the two large logs with IDs 6 and 3 were successfully detected. However, the logs with IDs 7, 8, and 9, located on the ground, were only partially detected. Specifically, only log 7 was detected by the TLS method. This limitation can be explained as follows: In the initial processing step, logs 8 and 9 were also detected but classified as a single segment because they converge at a certain point. As a result, this combined segment was assigned a broader width and did not meet the R^2 threshold defined in the methodology. Consequently, this segment was discarded. Examining Figure 6.1a, we observe that the program correctly detected logs 2 and 3 as separate entities, and log 4 was also accurately identified. However, log 19, which is not clearly visible in the image, was only partially detected. This may be due to the presence of branches along the log, which likely interfered with the algorithm's performance.

Next, we examine plot 610, which, as observed in the results section, produced particularly poor detection results. In this section, our aim is to understand the reasons behind this result. By analyzing the Figures 6.2, we observe that the plot 610 is characterized by a denser forest with significant understory, numerous small trees, and fallen logs that lie closer to the ground. In addition, many of these logs are heavily overgrown with moss, fungi, and other vegetation. This overgrowth affects the smoothness of the log surfaces, which poses challenges to the normal vector calculation and limits the effectiveness of the TLS-based method. Furthermore, as noted in the results section, a large portion of the ground surface of the plot was not successfully filtered during the initial steps of DTM generation, point cloud normalization, and the subsequent filtering process. This failure to remove ground points further contributed to poor detection performance.

In Figure 6.2a, we see the logs with IDs 10 and 11. These logs could not be detected using the TLS method. Similarly, the ULS method also failed to identify these logs. In Figure 6.2b, we observe logs with IDs 17, 15, 20, 21, 18, 19, 16, and 14. Here, the logs were only partially detected. For example, logs 17 and 15 were identified as a single segment using the TLS method, and log 16 was successfully detected. However, the smaller logs in the foreground of Figure 6.2b could not be identified using this TLS approach. Interestingly, the ULS method performed better in detecting these smaller logs, as seen in Figure 5.2c. This is particularly evident in the lower left corner of the plot, where the ULS method showed superior detection capabilities compared to TLS.

Finally, we analyze plot D3, which was selected due to its challenging characteristics. This plot contains numerous logs lying side by side, overlapping each other and featuring large

Figure 6.1: Pictures of Plot 611 with SegmentID (red)

branches and varying dimensions, making detection particularly complex (Figure 6.3).
Log ID 3, the largest log in the plot, lies directly on the ground. Adjacent to log ID 3, log ID 4 runs almost parallel to it but has a smaller diameter. Above both logs lies log ID 5. Referring to the results presented in Chapter 5 (Figure 5.3), we observe that log ID 3 was almost entirely undetected, while logs ID 4 and ID 5 were at least partially detected. This discrepancy may be explained by the TLS evaluation method, which uses only the highest and lowest points within a cell at any given time. As a result, many points from log ID 3 are lost during processing, preventing its full detection. The log with ID 7, which contributes significantly to the deadwood volume for plot D3, was unfortunately identified as an outlier. This classification occurred because the diameter determined for this log exceeded the predefined threshold.
Overall, across all plots, it can be observed that logs with very small diameters are also more difficult to detect. For example, in plot D3, logs with IDs 6 and 2 were poorly detected (Figure 5.3), likely due to their small size and reduced point density in the TLS data. Table 5.5 compares the volume of dead wood (in cubic meters) determined by the TLS method with

Figure 6.2: Pictures of Plot 610 with SegmentID (red)

the manual measurements across the different plots. At first glance, it appears that the TLS method closely approximates the manual values, especially for plot 611. However, this is not consistently the case for all plots.

For plot 611, the volume derived from TLS is reliable and aligns well with manual measurements. In contrast, the values for plot 610 should be interpreted with caution. Although the deviation between TLS and manual measurements is relatively small, this appears to be coincidental rather than indicative of accurate detection. Finally, for plot D3, the TLS values are more trustworthy and provide a reasonable approximation of the manual measurements. In summary, while the TLS method shows promising results in some plots, such as 611 and D3, the values for plot 610 cannot be considered reliable and are likely the result of chance. It is important to note that achieving good coverage with the TLS method requires multiple scanning positions, which involves a significant investment of time and equipment. In areas

Figure 6.3: Pictures of Plot D3 with SegmentID (red)

with only a small amount of deadwood, the time required for data collection using TLS is almost equivalent to that of manual measurements. However, in regions with a high density of deadwood, where manual measurements would be highly time consuming, the TLS method could be a valuable alternative due to its efficiency in capturing large volumes of data.

6.2. Comparison between Methods

In this section, we compare the results of the different methods for calculating the deadwood volume for each plot. A significant variation is observed in the volumes calculated using the different methods (Table 5.5). These 3 plots were specifically selected based on their deadwood content to test and validate the TLS method. From a visual analysis perspective, it can be observed that the ULS method performed well in detecting large logs and provided robust volume estimations compared to the TLS method (see Figures 5.1, 5.2 and 5.3). However, the ULS approach significantly underestimated the volume with only 22% of deadwood volume (Table 5.5). Lindberg et al., 2013 tested their method under comparable conditions and achieved 32% completeness. Nyström et al., 2014 achieved quite better results with 40% of trees detected. Comparison between studies is challenging due to the varying methodologies employed. Furthermore, differences in data collection methods, such as the resolution

of point clouds or the density of the scanned forest environment, further complicate comparability. The results of Mücke et al., 2013 corresponded to 41% of the stems measured in the field.

Under favorable conditions, the TLS method detected a greater number of smaller stems and was able to estimate their volume. Additionally, the ULS method is far less invasive in the field and significantly less time consuming than the TLS method. The Line Intersect method is also invasive, but requires less expensive equipment and can be carried out by any trained individual. Although it is slightly more time consuming than the ULS method, it is comparable in time requirements to the TLS method. Furthermore, data processing for the Line Intersect method is less complex and time consuming compared to the TLS method, which requires data referencing and extensive processing.

In this case, the line intersect method underestimated the deadwood volume in the plots. However, the results are highly dependent on the included tree stems. It is also recommended to apply this method to a larger number of plots and with a significantly larger radius (Wagner, 1968).

The results for dense forest areas, such as plot 610, highlight challenges for both the ULS and the TLS methods. In plot D3, both the ULS and the TLS methods slightly underestimated the manual measurements, probably influenced by the unique characteristics of this plot. Here, the line intersect method successfully captured all relevant logs, resulting in remarkably accurate outcomes. On the other hand, for plot 611, the TLS method outperformed the other methods, providing more accurate results.

7. Conclusion and Outlook

This study investigated different methods for assessing deadwood in an unmanaged forest (Rohrach Biosphere Reserve): manual measurements, the line intersect method, terrestrial laser scanning (TLS) and UAV-based laser scanning (ULS). A new approach was also developed to detect deadwood using TLS data, and its performance was thoroughly evaluated. The new TLS-based detection method proved to be effective in many cases. It performed well in identifying and measuring deadwood, particularly in areas where the logs were clearly visible and did not overlap. The method accurately calculated parameters such as volume, length, and diameter. However, it faced challenges in more complex scenarios, such as overlapping logs, logs partially covered by vegetation, or fragmented logs. These conditions caused errors in segmentation or led to the detection of logs that were not present. Compared to TLS, ULS demonstrated the ability to cover larger areas efficiently, making it suitable for large-scale assessments. However, ULS struggled in areas with dense vegetation or steep slopes, which caused underestimations of deadwood volume. Manual measurements remained the most accurate method for measuring deadwood but were too time- and labor-intensive for larger plots. The Line Intersect Method, while fast and simple, may be less reliable in areas where deadwood was unevenly distributed. This study highlights the potential of integrating the new TLS method with ULS to combine their respective strengths. Such an integrated approach could provide high precision on a local scale, while also effectively covering larger areas. For future research, the TLS detection algorithm should be refined to better handle complex forest conditions such as overlapping logs and fragmented data. Further studies should also explore ways to combine TLS and ULS datasets more effectively to create standardized protocols for deadwood monitoring.

Improving these methods is essential for sustainable forest management and conservation of biodiversity, especially in unmanaged forests. These advances will help improve the accuracy and efficiency of deadwood assessments and support long-term ecological studies.

A. Appendix: Opals Batch Code

```
rem Detection of deadwood

rem set file name
set fn=611_1cm
rem set working directory
cd E:\Opals_Data\611
set fn_sc=E:\Opals_Data\scripts

rem set working directory
cd D:\Opals_Data\611
set fn_sc=D:\Opals_Data\scripts

rem import Data
opalsimport -inf %fn%_EPSG25832.laz -outf %fn%.odm -tilesize 1
::opalsimport -inf %fn%.las -tilesize 1

_setCRS -inFile %fn%.odm  -epsgCode 25832

rem 1. DTM generation

rem limits 611
opalsexport -inf %fn%.odm -outf %fn%_limit.odm -limit 560927  5270728 560955  5270761 -tilesize 0.5
rem limits 610
::opalsexport -inf %fn%.odm -outf %fn%_limit.odm -limit 561027  5270730 561054  5270761 -filter "
    generic[Z < 655]" -tilesize 0.5
rem limits D3
::opalsexport -inf %fn%.odm -outf %fn%_limit.odm -limit 560935  5270772 560959  5270795 -tilesize 0.5

rem thinning - lowest last echo within 0.1 m cells as basis for DTM calculation
opalscell -inf %fn%_limit.odm -outf %fn%_min01.odm -cellsize 0.2 -feat min -filter echo[first]

rem hierarchical iterativ approach
opalscell -inf %fn%_min01.odm -outf %fn%_min3.odm -cellsize 1 -feat quantile:0.1
opalsgrid -inf %fn%_min01.odm -outf %fn%_min1_tr.tif -interpol delaunayTriangulation -grids 0.5 -
    searchRad 5
opalsfillgaps -inf %fn%_min1_tr.tif  -outFile %fn%_min1_tr_fg.tif -method triangulation
opalsaddinfo -inf %fn%_min01.odm  -gridf %fn%_min1_tr_fg.tif -attribute "normalizedZ=z-r[0]"

opalsGrid -inf %fn%_min01.odm -outFile %fn%_DTM2.tif -interpolation movingPlanes -grids 0.5 -searchRad
     3 -neighb 50 -filter "generic[normalizedz<1 and normalizedz>-2]"
opalsfillgaps -inf %fn%_DTM2.tif  -outFile %fn%_DTM2_fg.tif -method triangulation
opalsaddinfo -inf %fn%_min01.odm  -gridf %fn%_DTM2_fg.tif -attribute "normalizedZ=z-r[0]" -searchr 10

opalsGrid -inf %fn%_min01.odm -outFile %fn%_DTM3.tif -interpolation movingPlanes -grids 0.25 -
    searchRad 2 -neighb 10 -filter "generic[normalizedz<0.35 and normalizedz>-0.35]"
opalsfillgaps -inf %fn%_DTM3.tif  -outFile %fn%_DTM3_fg.tif -method triangulation
opalsaddinfo -inf %fn%_min01.odm  -gridf %fn%_DTM3_fg.tif -attribute "normalizedZ=z-r[0]" -searchr 10

opalsGrid -inf %fn%_min01.odm -outFile %fn%_DTM4.tif -interpolation movingPlanes -grids 0.2 -searchRad
     1 -neighb 10 -filter "generic[normalizedz<0.2 and normalizedz>-0.15]"
opalsfillgaps -inf %fn%_DTM4.tif  -outFile %fn%_DTM4_fg.tif -method triangulation
opalsaddinfo -inf %fn%_min01.odm  -gridf %fn%_DTM4_fg.tif -attribute "normalizedZ=z-r[0]" -searchr 10

opalsGrid -inf %fn%_min01.odm -outFile %fn%_DTM4.tif -interpolation movingPlanes -grids 0.15 -
    searchRad 0.5 -neighb 10 -filter "generic[normalizedz<0.1 normalizedz>0]"
opalsfillgaps -inf %fn%_DTM4.tif  -outFile %fn%_DTM.tif -method triangulation

opalsShade -inf %fn%_DTM.tif

rem 2. normalizing point cloud with the DTM
opalsaddinfo -inf %fn%_limit.odm  -gridf %fn%_DTM.tif -attribute "normalizedZ=z-r[0]"

rem 3. filter pointcloud between 0.1 and 4 meters above ground
opalsexport -inf %fn%_limit.odm -outf %fn%_sub_dw.odm  -filter "generic[normalizedz > 0.1 and
    normalizedz<4] and echo[first]"  -tilesize 0.5

rem 4. Calculate Distance to Plot Center 611
opalsaddinfo -inf %fn%_sub_dw.odm -attr "_dist2center=sqrt((X - 560941)*(X -560941) + (Y - 5270744)*(Y
     - 5270744))"

rem 5. filter all points outside 12m radius
opalsexport -inf %fn%_sub_dw.odm -outf %fn%_sub_dw2.odm -filter "generic[_dist2center < 12]" -tilesize
     0.5
```

```
65
66
67
68  rem Segemnatation for Deadwood
69  rem 6. Calculate Normals
70  opalsNormals -inf %fn%_sub_dw2.odm -storeMetaInfo maximum -neighb 50 -searchMode d3 -searchRadius 0.2
71
72  rem 7. Claculate linearity
73  opalsAddInfo -inf %fn%_sub_dw2.odm -attribute "_linearity(float)=sqrt(1-NormalEigenValue2/
        NormalEigenValue1)"
74
75  rem 8. filter NormalSigma0, NormalEigenvalue1,NormalEigenvalue2 and linearity after visual inspection
76  rem 611
77  opalsexport -inf  %fn%_sub_dw2.odm -outf %fn%_sub_dw3.odm  -filter "generic[NormalSigma0 < 0.012 and
        NormalEigenvalue1 < 0.04 and NormalEigenvalue2 < 0.025 and _linearity < 0.5]" -tilesize 0.5
78  rem 610
79  ::opalsexport -inf  %fn%_sub_dw2.odm -outf %fn%_sub_dw3.odm  -filter "generic[NormalSigma0 < 0.014 and
        NormalEigenvalue1 < 0.025 and NormalEigenvalue2 < 0.016 and _linearity < 0.6 and normalizedz <
        1.5]" -tilesize 0.5
80  rem D3
81  ::opalsexport -inf  %fn%_sub_dw2.odm -outf %fn%_sub_dw3.odm  -filter "generic[NormalSigma0 < 0.012 and
        NormalEigenvalue1 < 0.04 and _linearity < 0.6]" -tilesize 0.5
82
83
84  rem 9. select 0.1 and 0.9 z-Quantile per cell and combine
85  opalscell -inf %fn%_sub_dw3.odm -outf %fn%_sub_dw3_max.odm -cellsize 0.02 -feat quantile:0.9
86  opalscell -inf %fn%_sub_dw3.odm -outf %fn%_sub_dw3_min.odm -cellsize 0.02 -feat quantile:0.1
87  opalsexport -inf %fn%_sub_dw3_min.odm %fn%_sub_dw3_max.odm -outf %fn%_sub_dw3_comb.odm
88
89
90  rem 10. calculate 3D distance to the nearest neighbours
91  opalsaddinfo -inf %fn%_sub_dw3_comb.odm  -searchradius 1  -searchmod d3 -neighb 3  -attr "_p3dist=
        SqrDist3D(n[0], n[1])"
92
93  rem 11. normalize the compbined point cloud
94  opalsaddinfo -inf %fn%_sub_dw3_comb.odm  -gridf %fn%_DTM.tif -attribute "normalizedZ=z-r[0]"
95
96  rem 12. Calculate Normals and linearity
97  opalsNormals -inf %fn%_sub_dw3_comb.odm -storeMetaInfo maximum -neighb 50 -searchMode d3 -searchRadius
        0.1
98  opalsAddInfo -inf %fn%_sub_dw3_comb.odm -attribute "_linearity(float)=sqrt(1-NormalEigenValue2/
        NormalEigenValue1)"
99
100 rem 13. filter points of distance to neighbours and linearity
101 opalsexport -inf  %fn%_sub_dw3_comb.odm -outf %fn%_sub_dw4.odm -filter "generic[_p3dist < 0.001 and
        _linearity < 0.65]"
102
103 rem 14. Segmentation of lying deadwood
104 opalsSegmentation -inf %fn%_sub_dw4.odm -searchRadius 0.18 -searchMode d3 -minSegSize 300 -method
        condClustering -criterion "abs(_NormalEigenvector1X*n[0]._NormalEigenvector1X +
        _NormalEigenvector1Y*n[0]._NormalEigenvector1Y +_NormalEigenvector1Z*n[0]._NormalEigenvector1Z)>
        cos(0.06)"
105
106 rem 15. Filter every point which is not part of the a segment
107 opalsexport -inf %fn%_sub_dw4.odm -outf %fn%_seg.odm -filter "generic[SegmentID >= 0]"
108
109 rem calculates pdens and pcount map for visualizing
110 opalscell -inf %fn%_seg.odm -feature pdens pcount -cellSize 0.05
111
112 rem 16. export file as txt-file
113 opalsexport -inf %fn%_seg.odm  -outf %fn%_seg.txt -oformat %fn_sc%\output_dw.xml
114
115 rem 17. Python-Script for fitting polyline
116 rem imput-file; Results per Segment; Shapefile; Extended Pointcloud; Grad of fittet line, R^2-limit;
        lower-quantile; upper-quantile for diameter.
117 python %fn_sc%\ransac_poly.py %fn%_seg.txt %fn%_seg_attribute.txt %fn%_shapefile1.shp %fn%_shapefile2.
        shp %fn%_extended.txt 2 0.5 0.15 0.8
118
119 rem 18. Import extendet pointcloud
120 opalsimport -inf  %fn%_extended.txt -iformat %fn_sc%\import_ransac.xml  -outf %fn%_extended.odm
```

B. Appendix: Python Code

```python
import sys
import pandas as pd
import numpy as np
from sklearn.linear_model import RANSACRegressor
from sklearn.preprocessing import PolynomialFeatures
from sklearn.pipeline import make_pipeline
from sklearn.linear_model import LinearRegression
from sklearn.metrics import r2_score
from scipy.spatial.distance import euclidean
from scipy.integrate import quad
import shapefile  # PyShp for creating Shapefile output
import math

# Calculate Euclidean distance between two points
def calculate_distance(point1, point2):
    return euclidean(point1, point2)

# Calculate the tangent vector at the endpoint of the polynomial curve
def calculate_tangent(model, x_val):
    pipeline_model = model.estimator_
    poly_features = pipeline_model.named_steps['polynomialfeatures']
    lin_reg = pipeline_model.named_steps['linearregression']
    coefs = lin_reg.coef_
    degree = poly_features.degree
    derivative = sum(coefs[i] * i * (x_val ** (i - 1)) for i in range(1, degree + 1))
    return derivative

# Calculate the angle between two vectors
def calculate_angle_between_vectors(vec1, vec2):
    unit_vec1 = vec1 / np.linalg.norm(vec1)
    unit_vec2 = vec2 / np.linalg.norm(vec2)
    dot_product = np.dot(unit_vec1, unit_vec2)
    angle = np.arccos(dot_product)
    return np.degrees(angle)

# Generate points along the polynomial curve predicted by the RANSAC model
def get_polynomial_curve(ransac_model, x_min, x_max, num_points=100):
    x_values = np.linspace(x_min, x_max, num_points)
    y_values = ransac_model.predict(x_values.reshape(-1, 1))
    points = [(x_values[i], y_values[i]) for i in range(len(x_values))]
    return points

# Calculate the arc length of the polynomial curve between two x-values
def calculate_arc_length(ransac_model, x_min, x_max):
    arc_length_integral = lambda x: np.sqrt(1 + calculate_tangent(ransac_model, x)**2)
    arc_length, _ = quad(arc_length_integral, x_min, x_max)
    return arc_length

# Merge segments if they are close, similarly oriented, and at similar Z height
def merge_segments_if_similar(segments, distance_threshold=1.5, angle_threshold=15, z_threshold=0.3):
    merged_segments = []
    used_segments = set()

    for i, seg1 in enumerate(segments):
        if i in used_segments:
            continue

        current_merged_segment = seg1
        used_segments.add(i)
        current_merged_points = seg1['points']  # Collect points for post-merge RANSAC

        for j, seg2 in enumerate(segments):
            if j in used_segments or i == j:
                continue

            min_x1, max_x1 = seg1['x_min'], seg1['x_max']
            min_x2, max_x2 = seg2['x_min'], seg2['x_max']
            end_point1 = (max_x1, seg1['model'].predict([[max_x1]])[0])
            start_point2 = (min_x2, seg2['model'].predict([[min_x2]])[0])

            # Calculate the distance and angle between segments
            distance = calculate_distance(end_point1, start_point2)

```

```
            if distance < distance_threshold:
                tangent1 = calculate_tangent(seg1['model'], max_x1)
                tangent2 = calculate_tangent(seg2['model'], min_x2)
                angle = calculate_angle_between_vectors(np.array([1, tangent1]), np.array([1, tangent2
                    ]))

                # Pr fen der Z-H he der Segment-Endpunkte, wenn Werte vorhanden sind
                z_end1_points = seg1['points'][seg1['points'][:, 0] == max_x1]
                z_start2_points = seg2['points'][seg2['points'][:, 0] == min_x2]

                # Sicherstellen, dass z_end1 und z_start2 Werte enthalten, bevor darauf zugegriffen
                    wird
                if z_end1_points.size > 0 and z_start2_points.size > 0:
                    z_end1 = z_end1_points[0, 2]
                    z_start2 = z_start2_points[0, 2]
                    z_difference = abs(z_end1 - z_start2)

                    # Pr fen, ob der Z-H henunterschied innerhalb der Toleranz liegt
                    if angle < angle_threshold and z_difference < z_threshold:
                        # Add points of seg2 to the current merged points
                        current_merged_points = np.vstack([current_merged_points, seg2['points']])
                        current_merged_segment['x_min'] = min(current_merged_segment['x_min'], seg2['
                            x_min'])
                        current_merged_segment['x_max'] = max(current_merged_segment['x_max'], seg2['
                            x_max'])
                        used_segments.add(j)
                else:
                    # Falls keine passenden Z-Werte vorhanden sind, wird das Segment   bersprungen
                    continue


        # Update merged segment with all merged points
        current_merged_segment['points'] = current_merged_points
        merged_segments.append(current_merged_segment)

    return merged_segments

# Main RANSAC function with initial and post-merge Shapefile outputs
def ransac(input_file, output_file, initial_shapefile_output, merged_shapefile_output,
    text_output_file, degree, r2_threshold, quantile_lower, quantile_upper):
    point_cloud = pd.read_csv(input_file, delim_whitespace=True, names=['X', 'Y', 'Z', 'NormalizedZ',
        'SegmentID'], skiprows=1)
    segments = point_cloud.groupby('SegmentID')

    segment_results = []
    extended_points = []  # Temporary list for points from all segments
    filtered_extended_points = []  # Final list to store only points from accepted segments
    segment_info = []  # Store segment information for merging later

    # Initial Shapefile for segments after Step 2
    shp_initial = shapefile.Writer(initial_shapefile_output, shapeType=shapefile.POLYLINE)
    shp_initial.field('SegmentID', 'N')

    # Apply initial RANSAC to each segment and save to initial Shapefile
    for segment_id, segment in segments:
        X = segment[['X']].values
        y = segment['Y'].values

        pipeline_model = make_pipeline(PolynomialFeatures(degree), LinearRegression())
        ransac = RANSACRegressor(pipeline_model)
        ransac.fit(X, y)

        min_x, max_x = segment['X'].min(), segment['X'].max()

        # Save the fitted line as a polyline to the initial Shapefile
        initial_curve_points = get_polynomial_curve(ransac, min_x, max_x)
        shp_initial.line([initial_curve_points])
        shp_initial.record(SegmentID=segment_id)

        # Speichern von Segmentinformationen zum sp teren Merging
        segment_info.append({
            'SegmentID': segment_id,
            'model': ransac,
            'points': np.column_stack([X, y, segment['Z'].values]),  # Z-Koordinate hinzuf gen
            'x_min': min_x,
            'x_max': max_x
```

```
        })


        # Collect extended point data for each point in this segment
        for i in range(len(X)):
            extended_points.append({
                'X': segment.iloc[i]['X'],
                'Y': segment.iloc[i]['Y'],
                'Z': segment.iloc[i]['Z'],
                'SegmentID': segment_id,
                'Length': None,  # Placeholder for now, to be filled in Step 5
                'Diameter': None,  # Placeholder for now, to be filled in Step 5
                'Volume': None,  # Placeholder for now, to be filled in Step 5
                'Mean_Residual': None  # Placeholder for now, to be filled in Step 5
            })

    # Close the initial Shapefile
    shp_initial.close()

    # Merge segments and reapply RANSAC, then save merged Shapefile
    merged_segments = merge_segments_if_similar(segment_info)

    shp_merged = shapefile.Writer(merged_shapefile_output, shapeType=shapefile.POLYLINE)
    shp_merged.field('SegmentID', 'N')
    shp_merged.field('Length', 'F', decimal=8)
    shp_merged.field('Diameter', 'F', decimal=8)
    shp_merged.field('Volume', 'F', decimal=8)

    new_segment_id = 0
    for merged_segment in merged_segments:
        new_segment_id += 1
        merged_points = merged_segment['points']
        X_merged = merged_points[:, 0].reshape(-1, 1)
        y_merged = merged_points[:, 1]

        # Apply RANSAC again to the merged segment
        pipeline_model = make_pipeline(PolynomialFeatures(degree), LinearRegression())
        ransac = RANSACRegressor(pipeline_model)
        ransac.fit(X_merged, y_merged)

        # Calculate R   for quality assurance
        y_pred = ransac.predict(X_merged)
        r2 = r2_score(y_merged, y_pred)
        if r2 < r2_threshold:
            continue  # Skip segments that don't meet R   threshold

        # Calculate final length, diameter, and volume
        min_x, max_x = X_merged.min(), X_merged.max()
        residuals = y_merged - y_pred
        arc_length = calculate_arc_length(ransac, min_x, max_x)
        min_z = point_cloud[(point_cloud['X'] == min_x)]['Z'].values[0]
        max_z = point_cloud[(point_cloud['X'] == max_x)]['Z'].values[0]
        delta_z = max_z - min_z
        actual_length = math.sqrt(arc_length**2 + delta_z**2)
        q_lower = np.quantile(residuals, quantile_lower)
        q_upper = np.quantile(residuals, quantile_upper)
        diameter = abs(q_upper - q_lower)
        volume = math.pi * (diameter / 2) ** 2 * actual_length

        # Append segment results
        segment_results.append({
            'SegmentID': new_segment_id,
            'Length': actual_length,
            'Diameter': diameter,
            'Volume': volume,
            'Mean_Residual': residuals.mean()
        })

        # Add only accepted segment points to filtered list
        for point in extended_points:
            if point['SegmentID'] == merged_segment['SegmentID']:
                point['Length'] = actual_length
                point['Diameter'] = diameter
                point['Volume'] = volume
                point['Mean_Residual'] = residuals.mean()
                filtered_extended_points.append(point)
```

```
220
221         # Save merged segment to Shapefile
222         merged_curve_points = get_polynomial_curve(ransac, min_x, max_x)
223         shp_merged.line([merged_curve_points])
224         shp_merged.record(SegmentID=new_segment_id, Length=actual_length, Diameter=diameter, Volume=
                volume)
225
226     # Close the merged Shapefile
227     shp_merged.close()
228
229     # Save results to CSV and extended point cloud
230     results_df = pd.DataFrame(segment_results)
231     if not results_df.empty:
232         results_df.to_csv(output_file, index=False)
233     else:
234         print("Warning: No data in segment_results to save in output file.")
235
236     # Only save points in accepted segments to the extended output
237     filtered_extended_points_df = pd.DataFrame(filtered_extended_points)
238     if not filtered_extended_points_df.empty:
239         filtered_extended_points_df.to_csv(text_output_file, sep=' ', index=False)
240     else:
241         print("Warning: No data in filtered_extended_points to save in text output file.")
242
243     # Print the total number of final segments that passed quality assurance
244     print(f"Total number of final segments: {len(segment_results)}")
245     print(f"Initial Shapefile saved as {initial_shapefile_output}")
246     print(f"Merged Shapefile saved as {merged_shapefile_output}")
247     print(f"Results saved in {output_file}")
248     print(f"Extended point information saved in {text_output_file}")
249
250 if __name__ == "__main__":
251     ransac(sys.argv[1], sys.argv[2], sys.argv[3], sys.argv[4], sys.argv[5], degree=int(sys.argv[6]),
252            r2_threshold=float(sys.argv[7]), quantile_lower=float(sys.argv[8]), quantile_upper=float(
                sys.argv[9]))
```

References

Cheng, C.-L., Shalabh, & Garg, G. (2014). Coefficient of determination for multiple measurement error models. *Journal of Multivariate Analysis*, *126*, 137–152. https://doi.org/https://doi.org/10.1016/j.jmva.2014.01.006

Fischler, M. A., & Bolles, R. C. (1981). Random sample consensus: A paradigm for model fitting with applications to image analysis and automated cartography [Place: New York, NY, USA Publisher: Association for Computing Machinery]. *Commun. ACM*, *24*(6), 381–395. https://doi.org/10.1145/358669.358692

Grabherr, G., & Broggi, M. (1999). *Ein Wald im Aufbruch: Das Naturwaldreservat Rohrach (Vorarlberg, österreich)*. Bristol-Stiftung. https://books.google.at/books?id=vCAqAAAACAAJ

Humphrey, J., Sippola, A., Lempérière, G., Dodelin, B., Alexander, K., & Butler, J. (2005). Deadwood as an indicator of biodiversity in European forests: From theory to operational guidance. *Monitoring and indicators of forest biodiversity in Europe–from ideas to operationality*, *51*, 193–206.

Kirchmeir, H., Steinbauer, K., Berger, V., Posch, L., Thaler, S., Rathke, H., Nussbaumer, D., Schimpl, L., & Hollaus, M. (2023). Digitale Bestanderfassung und Entwicklungsanalyse für das Naturwaldreservat Rohrach: E.C.O. Institut für ökologie, Klagenfurt, 39 S.

Liang, X., Hyyppä, J., Kaartinen, H., Lehtomäki, M., Pyörälä, J., Pfeifer, N., Holopainen, M., Brolly, G., Francesco, P., Hackenberg, J., Jinhu Wang, Huang, H., Jo, H.-W., Katoh, M., Liu, L., Mokroš, M., Morel, J., Olofsson, K., Jose Alejandro Poveda Lopez, . . . Wang, Y. (2018). International benchmarking of terrestrial laser scanning approaches for forest inventories [MAG ID: 2884197231]. *Isprs Journal of Photogrammetry and Remote Sensing*, *144*, 137–179. https://doi.org/10.1016/j.isprsjprs.2018.06.021

Lindberg, E., Hollaus, M., Mücke, W., Fransson, J., & Pfeifer, N. (2013). Detection of lying tree stems from airborne laser scanning data using a line template matching algorithm [MAG ID: 2114891033]. *ISPRS Annals of the Photogrammetry, Remote Sensing and Spatial Information Sciences*, 169–174. https://doi.org/10.5194/isprsannals-ii-5-w2-169-2013

Marchetti, M. (2004). Monitoring and Indicators of Forest Biodiversity in Europe - From Ideas to Operationality [MAG ID: 2338449464].

Marchi, N., Yang, B., Jinhu Wang, Wang, J., Pirotti, F., & Lingua, E. (2018). Airborne and Terrestrial Laser Scanning Data for the Assessment of Standing and Lying Deadwood: Current Situation and New Perspectives [MAG ID: 2889130004]. *Remote Sensing*, *10*(9), 1356. https://doi.org/10.3390/rs10091356

Melzer, T., & Briese, C. (2004). Extraction and Modeling of Power Lines from ALS Point Clouds.

Merganičová, K., Merganič, J., Svoboda, M., Bače, R., & Šebeň, V. (2012). Deadwood in Forest Ecosystems [MAG ID: 1566563689]. https://doi.org/10.5772/31003

Mücke, W., Deák, B., Schroiff, A., Hollaus, M., & Pfeifer, N. (2013). Detection of fallen trees in forested areas using small footprint airborne laser scanning data [MAG ID: 2059237486]. *Canadian Journal of Remote Sensing*, *39*. https://doi.org/10.5589/m13-013

Mücke, W., Hollaus, M., & Pfeifer, N. (2012). Identification of dead trees using small footprint full-waveform airborne laser scanning data [MAG ID: 2189103352].

Nyström, M., Holmgren, J., Fransson, J., J.E.S. Fransson, & Olsson, H. (2014). Detection of windthrown trees using airborne laser scanning [MAG ID: 2092681559]. *International Journal of Applied Earth Observation and Geoinformation*, *30*, 21–29. https://doi.org/10.1016/j.jag.2014.01.012

Paletto, A., Ferretti, F., De Meo, I., Cantiani, P., & Focacci, M. (2012). Ecological and Environmental Role of Deadwood in Managed and Unmanaged Forests [MAG ID: 1577481453 S2ID: 0c3fd038fae08c25547b34a9d490aea0f7fa5676]. https://doi.org/10.5772/24894

Pesonen, A., Matti Maltamo, Maltamo, M., Eerikäinen, K., & Packalén, P. (2008). Airborne laser scanning-based prediction of coarse woody debris volumes in a conservation area [MAG ID: 1996022982 S2ID: 007bfdd2135f8962d60acb042ccdfbb307398b2c]. *Forest Ecology and Management*, *255*(8), 3288–3296. https://doi.org/10.1016/j.foreco.2008.02.017

Pfeifer, N., Mandlburger, G., Otepka, J., & Karel, W. (2014). OPALS – A framework for Airborne Laser Scanning data analysis. *Computers, Environment and Urban Systems*, *45*, 125–136. https://doi.org/https://doi.org/10.1016/j.compenvurbsys.2013.11.002

Pfeifer, N., & Mandlburger, G. (2018). LiDAR data filtering and digital terrain model generation. In *Topographic laser ranging and scanning* (pp. 349–378). CRC Press.

Polewski, P., Yao, W., Heinrich, M., Krzystek, P., & Stilla, U. (2017). A voting-based statistical cylinder detection framework applied to fallen tree mapping in terrestrial laser scanning point clouds [MAG ID: 2613230219]. *Isprs Journal of Photogrammetry and Remote Sensing*, *129*, 118–130. https://doi.org/10.1016/j.isprsjprs.2017.04.023

Polewski, P., Yao, W., Heurich, M., Krzystek, P., & Stilla, U. (2015). Detection of fallen trees in ALS point clouds using a Normalized Cut approach trained by simulation [MAG ID: 2034933046]. *Isprs Journal of Photogrammetry and Remote Sensing*, *105*, 252–271. https://doi.org/10.1016/j.isprsjprs.2015.01.010

Stokland, J. N., Siitonen, J., & Jonsson, B. G. (2012). Biodiversity in dead wood. [MAG ID: 234454337].

Wagner, V. (1968). The Line Intersect Method in Forest Fuel Sampling [MAG ID: 172705342 S2ID: 3748a8fadb327577a7c233cf62b782d315218728]. *Forest Science*, *14*(1), 20–26. https://doi.org/10.1093/forestscience/14.1.20

Yrttimaa, T., Saarinen, N., Luoma, V., Tanhuanpää, T., Kankare, V., Liang, X., Hyyppä, J., Holopainen, M., & Vastaranta, M. (2019). Detecting and characterizing downed dead wood using terrestrial laser scanning [MAG ID: 2920797839]. *Isprs Journal of Photogrammetry and Remote Sensing*, *151*, 76–90. https://doi.org/10.1016/j.isprsjprs.2019.03.007

Yrttimaa, T., Wang, D., Saarinen, N., Luoma, V., Tanhuanpää, T., Kankare, V., Liang, X., Hyyppä, J., Holopainen, M., & Vastaranta, M. (2020). Terrestrial Laser Scanning and Ground Truth Data for Characterizing Downed Dead Wood [MAG ID: 4205332331 S2ID: 9f61118bf8b248db2935c04797a3ee83594fa58a]. https://doi.org/10.31219/osf.io/gz93a